Current Research in Food Science 10 (2025) 101051

Contents lists available at ScienceDirect

Current Research in Food Science

journal homepage: www.sciencedirect.com/journal/current-research-in-food-science

Lacticaseibacillus casei IDCC 3451 alleviates cognitive and behavioral functions by reshaping the gut microbiome and regulating intestinal barrier integrity in chronic stress animal models

Anna Kang [a,1], Ju Young Eor [a,1], Junbeom Lee [a,1], Min-Jin Kwak [a], Daniel Junpyo Lee [a], Eunsol Seo [a], Woong Ji Lee [a], Seon-hui Son [a], Minho Song [b], Jun-Mo Kim [c], Hyung Wook Kim [d], Jungwoo Yang [e], Sangnam Oh [f,*], Younghoon Kim [a,**]

[a] Department of Agricultural Biotechnology and Research Institute of Agriculture and Life Science, Seoul National University, Seoul, 08826, South Korea
[b] Department of Animal Science and Biotechnology, Chungnam National University, Daejeon, 34134, South Korea
[c] Department of Animal Science and Technology, Chung-Ang University, Anseong 17546, Gyeonggi-do, South Korea
[d] College of Life Sciences, Sejong University, Seoul, 05006, South Korea
[e] Department of Microbiology, College of Medicine, Dongguk University, Gyeongju, 38066, South Korea
[f] Department of Functional Food and Biotechnology, Jeonju University, Jeonju, 55069, South Korea

ARTICLE INFO

Handling Editor: Dr. Yeonhwa Park

Keywords:
C. elegans
L. casei
Probiotics
Gut–brain axis
Chronic stress
DSS-Induced colitis

ABSTRACT

Lacticaseibacillus casei IDCC 3451 (3451) was evaluated for its effects on the gut-brain axis using *Caenorhabditis elegans* (*C. elegans*) and mouse models of stress and inflammation. In *C. elegans*, 3451 extended lifespans by 25 %, improved motility, and chemotaxis, enhanced survival under pathogen challenge, and reduced amyloid beta accumulation by 42 %. Transcriptomic profiling revealed upregulation of genes involved in neurotransmitter signaling and serine/threonine pathways. In the unpredictable chronic mild stress (UCMS) mouse model, 3451 administration increased the time spent in the center of the open field by 65 % and reduced immobility in the forced swim test by 32 %, indicating anxiolytic and antidepressant effects. Serum levels of aspartate aminotransferase (AST) and gamma-glutamyl transferase (GGT) were decreased by 18 % and 24 %, respectively. Additionally, 3451 restored the expressions of 5HT1AR, GABAR, and tight junction proteins, including *ZO-1* and *Claudin1*. Metabolomic analysis showed increased glycine and decreased palmitic acid levels, associated with an increased abundance of *Ruminococcus* and *Akkermansia*. In the dextran sulfate sodium (DSS)-induced colitis model, 3451 reduced the disease activity index by 36 %, improved colon histology, increased goblet cell preservation, and upregulated *ZO-1* and IL-10 expression. Threonine levels were also increased and correlated with a higher abundance of *Coprococcus*. These findings demonstrate that 3451 improved behavioral and intestinal outcomes through coordinated modulation of host signaling, metabolite production, and gut microbial composition, highlighting its therapeutic potential for managing IBD and neurobehavioral disorders.

1. Introduction

Probiotics, defined as live microorganisms that confer health benefits to the host when administered in adequate amounts (Salminen et al., 2021; Li et al., 2025), have attracted growing scientific interest. Among them, lactic acid bacteria, particularly *Lactobacillus* species, have emerged as leading candidates due to their established roles in maintaining homeostasis, modulating immune responses, and supporting cognitive health (Gareau, 2016; van Baarlen et al., 2013). Numerous studies have demonstrated their potential in preventing or mitigating inflammatory bowel disease (IBD) and neurodegenerative disorders, including Alzheimer's disease (AD), and Parkinson's disease, and autism spectrum disorders (Sarowska et al., 2013; Umbrello and Esposito, 2016; Zhu et al., 2022). Recent research has expanded the understanding of how probiotics interact with the gut microbiota to influence host physiology, supported by an increasing number of genomic and

* Corresponding author.
** Corresponding author.
E-mail addresses: osangnam@jj.ac.kr (S. Oh), ykeys2584@snu.ac.kr (Y. Kim).
[1] These authors contributed equally to the manuscript.

https://doi.org/10.1016/j.crfs.2025.101051
Received 27 February 2025; Received in revised form 1 April 2025; Accepted 11 April 2025
Available online 14 April 2025
2665-9271/© 2025 The Authors. Published by Elsevier B.V. This is an open access article under the CC BY-NC-ND license (http://creativecommons.org/licenses/by-nc-nd/4.0/).

functional studies (Han et al., 2023; Kim et al., 2023a, 2023b, 2023c; Oh et al., 2022a; Park et al., 2023a, 2023b; Ryu et al., 2023; Yang et al., 2022; Yoo et al., 2022a).

Building on this foundation, a deeper understanding of host physiological changes is particularly important in the context of neurodegenerative diseases, which are driven by complex interactions involving aging, immune dysregulation, and chronic inflammation. Addressing these multifactorial processes requires an integrated approach, including the study of immune modulation, neuronal repair, and the regulation of disease-associated biomarkers. These mechanisms have been widely discussed in the context of aging and neuroinflammation (Minhas et al., 2021; Huang et al., 2018). Genetic and transcriptomic analyses play a crucial role in identifying molecular pathways that drive these phenotypic changes (Papassotiropoulos et al., 2006).

To investigate these mechanisms in a controlled and genetically tractable system, *Caenorhabditis elegans* (*C. elegans*) has emerged as a powerful model organism for studying aging, neurodegeneration, and host-microbe interactions. With its fully sequenced genome, short life cycle, and simple nervous system, *C. elegans* provides a high-throughput platform for analyzing physiological and behavioral traits (Brenner, 1974). The use of genetically modified strains has further enabled the investigation of specific pathological features, such as amyloid beta accumulation, locomotor dysfunction, immune response, and oxidative stress (Sonowal et al., 2017; Chu et al., 2022). While *C. elegans* may not fully replicate the complexity of mammalian systems, its efficiency in enabling mechanistic investigations into evolutionarily conserved pathways relevant to host-microbe interactions and neurodegenerative processes is unparalleled. This makes it a highly valuable screening model before validation in mammalian studies. Furthermore, *C. elegans* has found extensive use in modeling human diseases, such as metabolic disorders, obesity, and neurodegenerative conditions, thereby serving as a valuable alternative to mammalian models (Caldwell et al., 2020; Kumar et al., 2020). In microbiome research, *C. elegans* is increasingly used to evaluate probiotic effects on host physiology and disease progression. In this context, the present study first investigates the immunomodulatory and anti-aging properties of *Lacticaseibacillus casei* IDCC 3451 (3451) in *C. elegans*, focusing on its ability to reduce amyloid beta accumulation and ameliorate behavioral impairments associated with aging and neurodegeneration. 3451 is a relatively underexplored probiotic strain, with only two prior studies addressing its characteristics. One reported its genomic safety and distinctive enzymatic activities, such as high α-chymotrypsin activity and glucoside metabolism (Shin et al., 2021). The other demonstrated its ability to enhance plasma amino acid absorption when co-administered with plant-based proteins in mice (Kim et al., 2024). However, its role in systemic host physiology, especially within the gut–brain axis remains uncharacterized.

Moving beyond nematode models, chronic psychological stress has also been recognized as a major environmental risk factor for neuropsychiatric disorders. Stress-induced immune dysfunction and neuroinflammation are implicated in the pathophysiology of anxiety, depression, and cognitive decline (Dhabhar, 2014; Lupien et al., 2018). While antidepressants remain the first-line therapy, their limited efficacy in some cases has driven interest in microbiome-based interventions (Goodwin and Stein, 2021). Probiotics have shown potential in modulating brain function through gut-brain axis signaling, influencing neurotransmitter activity, inflammatory mediators, and behavioral responses (Forth et al., 2023; Ruan et al., 2023; Huang et al., 2024a; Gao et al., 2022). The gut microbiome plays a central role in maintaining intestinal barrier integrity and regulating host immune responses. Disruptions in microbial composition, commonly referred to as dysbiosis, can impair tight junction proteins, such as claudins and occludins, leading to increased intestinal permeability translocation of microbial products like lipopolysaccharides (LPS) into systemic circulation. These circulating pro-inflammatory mediators can access the central nervous system and promote neuroinflammation, ultimately contributing to behavioral abnormalities and cognitive dysfunction. This microbiota–gut–brain communication axis is increasingly recognized as a key regulator of neurophysiological processes and disease progression (Cryan et al., 2019; Obata and Pachnis, 2016).

Similarly, IBD, including ulcerative colitis and Crohn's disease, is characterized by relapsing intestinal inflammation driven by gut microbial dysbiosis, mucosal immune imbalance, and impaired epithelial barrier function. Although its precise etiology remains unclear, probiotics have demonstrated promising effects in modulating intestinal microbiota and improving barrier integrity, leading to symptom alleviated in colitis and related disorders (van Baarlen et al., 2013; Jaafar et al., 2023; Lee et al., 2022; Oh et al., 2022b; Yoo et al., 2022b; Liu et al., 2025). Furthermore, probiotics and microbial metabolites can influence host nutritional status and immune regulation (Jo et al., 2023; Kwak et al., 2023; Munezero et al., 2023; Vasquez et al., 2022; Pu et al., 2024).

To further explore the therapeutic potential of 3451 in modulating the gut-brain axis, we evaluated its effects in two murine models: the unpredictable chronic mild stress (UCMS) model of psychiatric dysfunction and the dextran sulfate sodium (DSS)-induced colitis model. A combination of behavioral assays, histological analysis, gene expression profiling, and integrated metagenomic and metabolomic assessments was employed to examine how 3451 influences host immunity, neuro-regulation, and intestinal health.

2. Results

2.1. Functional experiments using C. elegans

To assess the impact of strain 3451 on lifespan, survival assays were conducted in the *C. elegans* CF512 model. *Lactocaseibacillus rhamnosus* GG (LGG), a positive control group, significantly improved lifespan compared to the *Escherichia coli* OP50-fed group (*E. coli* OP50; OP50) ($p < 0.0001$). 3451 showed a significantly improved survival rate compared with *E. coli* OP50 ($p < 0.0001$) (Fig. 1A). To evaluate host resistance to foodborne pathogens, a killing assay was performed. Compared to *E. coli* OP50, 3451 ($p < 0.0001$) conferred greater protection against the Gram-positive bacterium *Staphylococcus aureus* Newman, with a higher survival rate than that conferred by LGG ($p < 0.0001$ vs. $p = 0.0001$, respectively) (Fig. 1B). Additionally, 3451 showed a significant protective effect against the Gram-negative pathogen *Escherichia coli* O157:H7 EDL933 ($p = 0.0355$), although the effect was less pronounced than that observed with LGG ($p = 0.0015$) (Fig. 1C).

Transcriptomic analysis was performed using Cytoscape to examine gene-level changes. The analysis indicated that genes regulated by 3451 were enriched in pathways associated with monooxygenase activity and nuclear receptor activity, monooxygenase activity, nuclear receptor signaling, G protein–coupled receptor activity, eating behavior, and myosin phosphatase regulation, which suggesting enhanced nervous system modulation (Fig. 1D). Collectively, these findings indicate that 3451 promotes the expression of genes involved in antimicrobial immunity, longevity regulation, and neural signaling. In particular, the upregulation of pathway related to serine and threonine activity suggests potential benefits in neurotransmission and lifespan extension.

2.2. Behavior and transcriptomic analysis of C. elegans

To assess the effects of the 3451 treatments on *C. elegans* behavior, motility, pharyngeal pumping, and sensory function were evaluated using CL4176 mutant strain, which accumulates amyloid beta, and CL2122 as the normal control. In the thrashing assay, both CL2122 and CL4176 strains exhibited significantly improved motility following treatment with 3451 compared to *E. coli* OP50-fed controls (CL2122: $p = 0.0138$, CL4176: $p = 0.0195$) (Fig. 2A and B). In the pharyngeal pumping assay, a significant increase in the number of pumps was observed in the CL4176 group on day 5 following 3451 administration

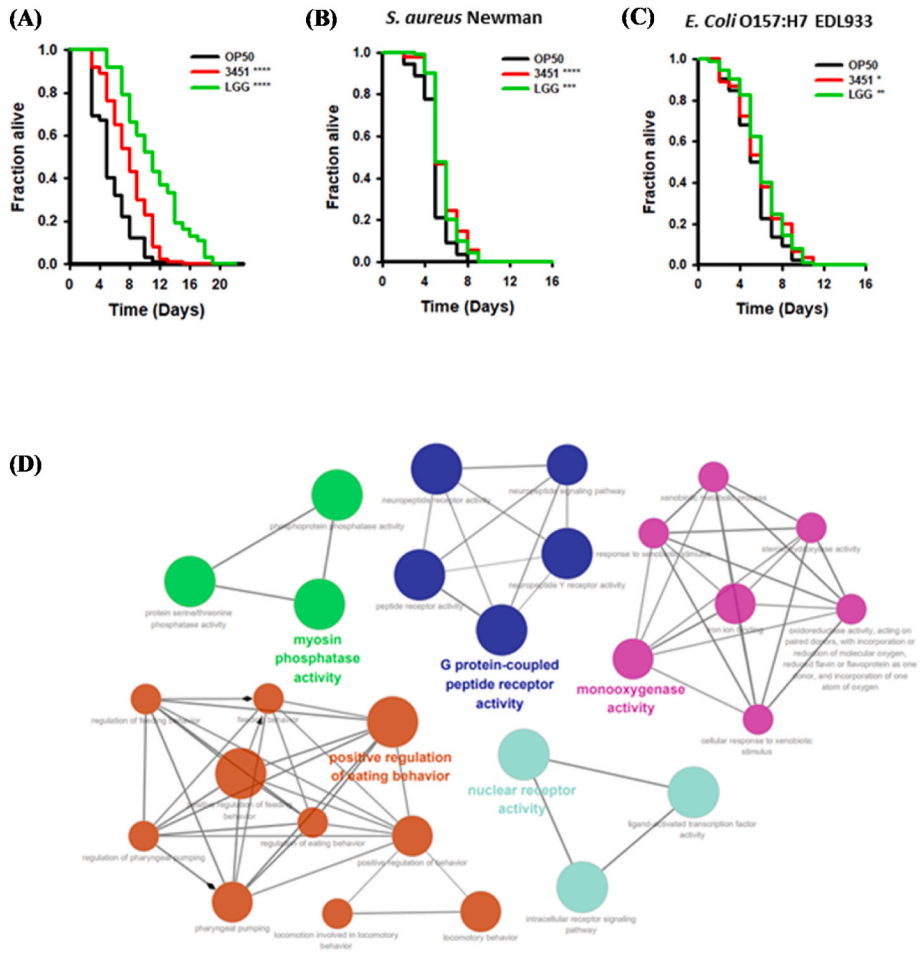

Fig. 1. Effect of *Lacticaseibacillus casei* IDCC 3451 on *C. elegans* (A) lifespan, pathogen killing assay using (B) *S. aureus* Newman, (C) *E. coli* O157:H7 EDL933 strains, and (D) transcriptomic analysis. *E. coli* OP50, normal control group; 3451, 3451 strain-treated group; LGG, positive control group. Results are expressed as mean $n = 30$ per group. *Means in the same series with significantly different (*, $p < 0.05$; **, $p < 0.01$; ***, $p < 0.001$; ****, $p < 0.0001$).

($p = 0.0112$), suggesting enhanced neuromuscular function (Fig. 2C and D). In the chemotaxis assay (Fig. 2E–H), 3451 treatment significantly increased attraction to attractants in CL2122 ($p = 0.0449$) and CL4176 ($p = 0.0353$) (Fig. 2E and F) and significantly less *C. elegans* directed to the repellent (CL2122: $p = 0.0024$, CL4176: $p = 0.0402$) (Fig. 2G and H). These behavioral improvements suggest that 3451 mitigates age- and amyloid beta-induced impairments in sensory perception and neural function.

Transcriptomic network analysis using Cytoscape indicated that genes modulated by 3451 were enriched in pathways related to monooxygenase activity, nuclear receptor signaling, and neural processes such as G protein–coupled receptor activity, eating behavior, and myosin phosphatase activity (Fig. 1D). Overall, these results suggest that 3451 promotes the expression of genes involved in antimicrobial defense, neural signaling, and lifespan extension, particularly through the enhancement of serine and threonine activity associated with neurotransmission.

2.3. Localization of amyloid beta in C. elegans

To evaluate the neuroprotective effects of 3451 strain and its influence on amyloid beta accumulation, GFP fluorescence imaging was conducted in *C. elegans* models. The CL2120 strain expresses GFP-tagged amyloid beta, and CL2122 serves as the control. In both strains, GFP fluorescence intensity was markedly reduced in worms treated with 3451 compared to *E. coli* OP50. ($p < 0.0001$) (Fig. 3A and B). Additionally, the GFP-positive area in CL2120 worms was significantly smaller in the 3451-treated group than in the *E. coli* OP50 group ($p = 0.0010$) (Fig. 3C and D). These results demonstrate that 3451 effectively reduces amyloid beta accumulation in transgenic *C. elegans* models of neurodegeneration.

2.4. Body weight and serum biochemical analysis in the UCMS model

Body weight was monitored to evaluate the general health and nutritional status of mice subjected to UCMS. At week 9, the CONT and LGG groups exhibited significantly higher body weights compared to the UCMS group ($p < 0.0001$, respectively). Although the 3451 group showed a trend toward increased body weight, the difference did not reach statistical significance (Fig. 5A). These findings suggest that UCMS reduces body weight gain, and that the administration of LGG or 3451 may attenuate this stress-induced effect.

In serum biochemical analysis, aspartate aminotransferase (AST) levels were significantly lower in the CONT, LGG, and 3451 groups compared to the UCMS group ($p = 0.0481$, $p = 0.0410$, and $p = 0.0180$, respectively) (Fig. 5B). Alanine aminotransferase (ALT) levels were significantly decreased in the CONT group than in the UCMS group ($p < 0.0001$). While the UCMS group exhibited elevated ALT levels, both the LGG and 3451 groups showed reduced levels (226.2 % in UCMS, 197.1 % in LGG, and 189.3 % in 3451), although the differences were not statistically significant (Fig. 5C). Gamma-glutamyl transferase (GGT) levels were also significantly lower in the CONT, LGG, and 3451 groups than in the UCMS group ($p = 0.0001$, $p = 0.0005$, and $p < 0.0001$, respectively) (Fig. 5D). These results suggest that UCMS induces

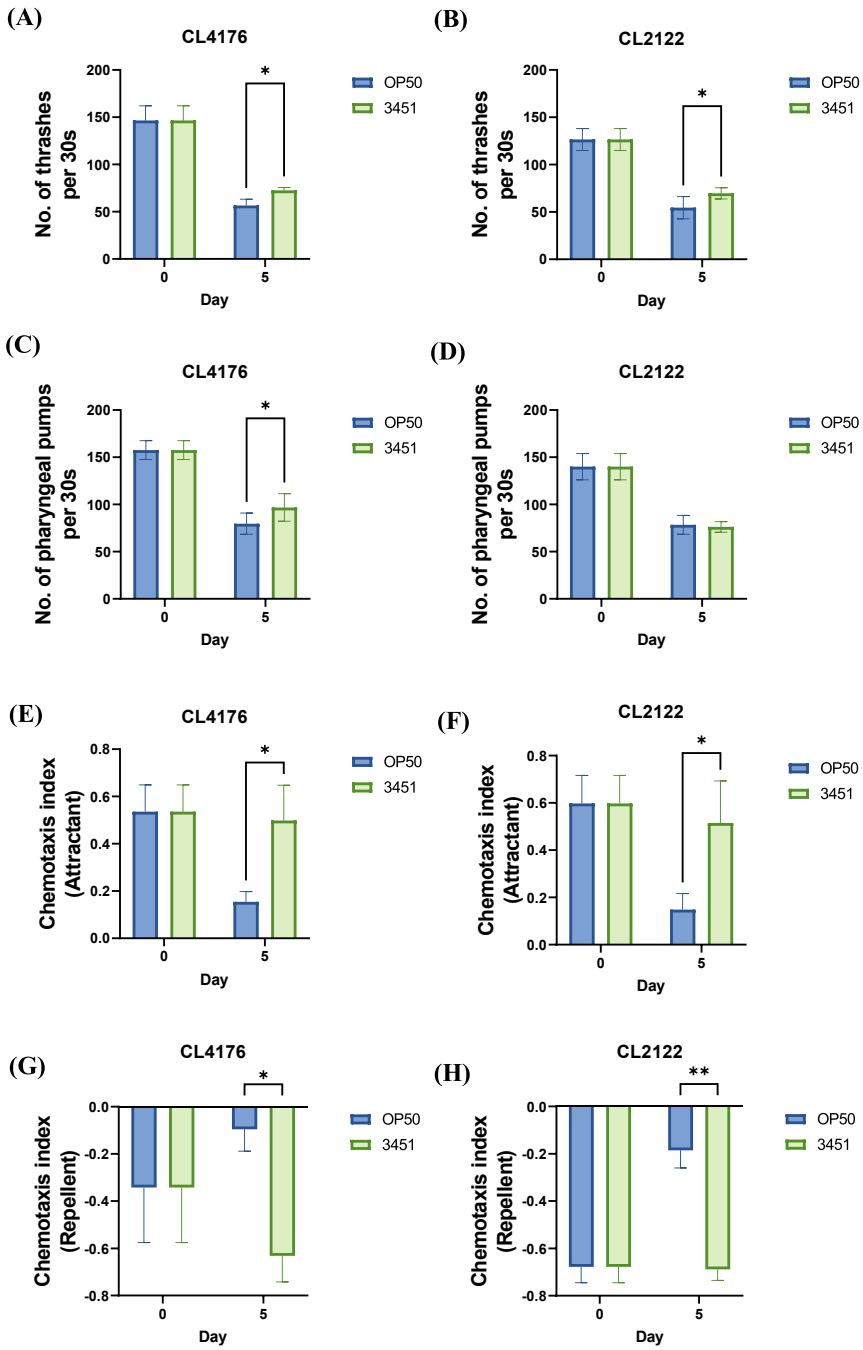

Fig. 2. Effect of *Lacticaseibacillus casei* IDCC 3451 on mutated *C. elegans* (CL4176, CL2122) behavior: (A–B) thrashing count for 30 s, (C–D) pharyngeal pumping count, and (E–H) chemotaxis index. Results are expressed as mean ± standard error mean (SEM); $n = 10$ per group. *Means in the same series with significantly different (*, $p < 0.05$; **, $p < 0.01$; ***, $p < 0.001$; ****, $p < 0.0001$).

systemic biochemical disturbances, and that 3451 administration may help mitigate stress-related hepatic and inflammatory changes.

2.5. Stress-related behavioral analysis in the UCMS model

To assess anxiety-like behavior in UCMS mice, the open field test (OFT) and elevated zero maze (EZM) were performed. From the OFT result, the UCMS group exhibited significantly reduced time spent and distance traveled in the center of the field compared to other groups (Fig. 6A and B), while time and distance spent in the corners were significantly increased (Suppl Figs. 1A–B). These results indicate heightened anxiety and diminished exploratory behavior induced by UCMS, which were ameliorated by LGG and 3451 treatment. In the EZM test, the UCMS group spent significantly less time in the open areas than the other groups (Fig. 6C) and traveled significantly shorter distances compared to the CONT group, with a decreasing trend compared to the LGG and 3451 groups (Suppl Fig. 1C). The number of entries into the open area was also significantly lower in the UCMS group than in the other groups (Fig. 6D).

Depression-like behaviors were assessed using the forced swim test (FST), tail suspension test (TST), and sucrose preference test (SPT). Immobility time in the FST and TST was significantly reduced in the

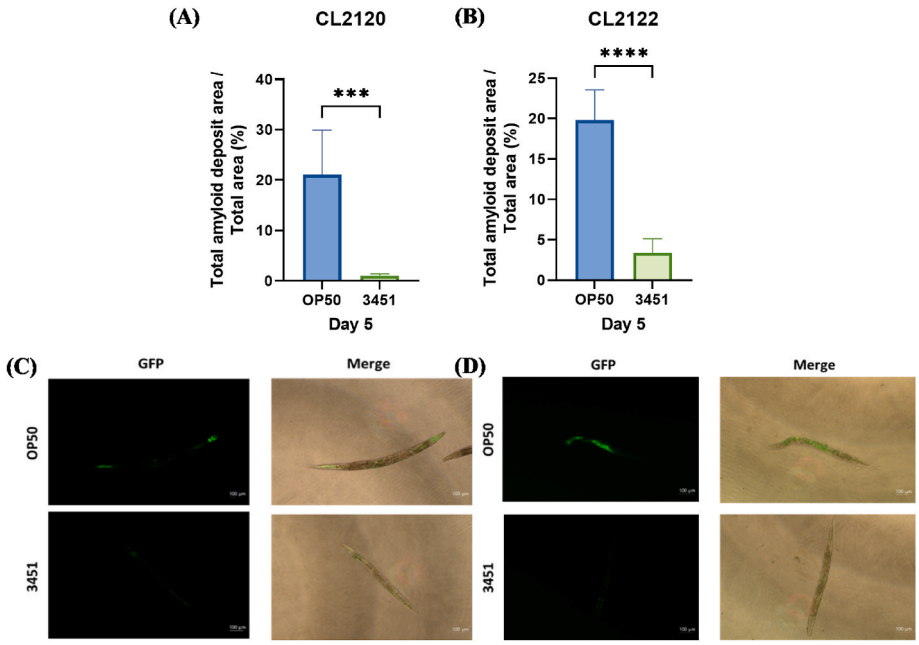

Fig. 3. Effect of *Lacticaseibacillus casei* IDCC 3451 on genetically mutated *C. elegans* (CL2120 and CL2122) in (A–B) amyloid beta accumulation ratio and (C–D) GFP fluorescence analysis. Results are expressed as mean ± standard error mean (SEM); $n = 5$ per group. *Means in the same series with significantly different (*, $p < 0.05$; **, $p < 0.01$; ***, $p < 0.001$; ****, $p < 0.0001$).

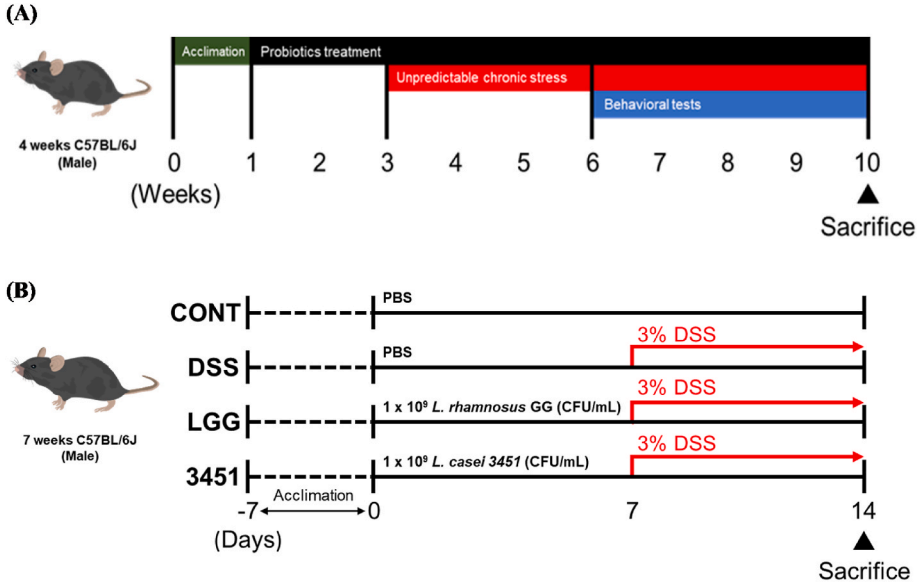

Fig. 4. Graphical scheme and timeline of conducted experiments. (A) UCMS animal experiment and **(B)** DSS-induced inflammation animal experiment models.

LGG- and 3451-treated groups relative to the UCMS group, indicating antidepressant-like effects (Fig. 6E and F). Furthermore, the decline in sucrose preference caused by UCMS was reversed in the LGG and 3451 groups (Fig. 6G).

Cognitive function was evaluated using the Y-maze and novel object recognition (NOR) tests. In the Y-maze, the UCMS group showed a significantly reduced number of spontaneous alternations, while LGG and 3451 treatment restored alternation performance (Fig. 6H). Total exploration time was also significantly decreased in the UCMS group compared to CONT and LGG (Fig. 6I). In the NOR test, the UCMS group did not show a preference for novel objects, whereas LGG and 3451 administrations led to a significant increase in time spent exploring novel objects, suggesting improved memory and recognition (Fig. 6J).

2.6. Correlation analysis for metagenome and metabolome in the UCMS model

To investigate the relationship between microbial shifts and metabolic changes following 3451 administration, integrated analysis of the gut microbiome and metabolome was performed in the UCMS model. Treatment with 3451 led to a significant increase in the relative abundance of *Coprococcus*, *Akkermansia*, *Ruminococcus*, *Parabacteroides*, and members of the *S24-7* family compared to the UCMS group (Fig. 7A). Metabolomic profiling revealed that levels of glycerol, L-glutamic acid, glycine, and L-leucine were significantly elevated, while palmitic acid levels were significantly reduced in the 3451 group compared to UCMS controls. In addition, dopamine, lactic acid, L-valine, and L-alanine showed increasing trends (Fig. 7C–K).

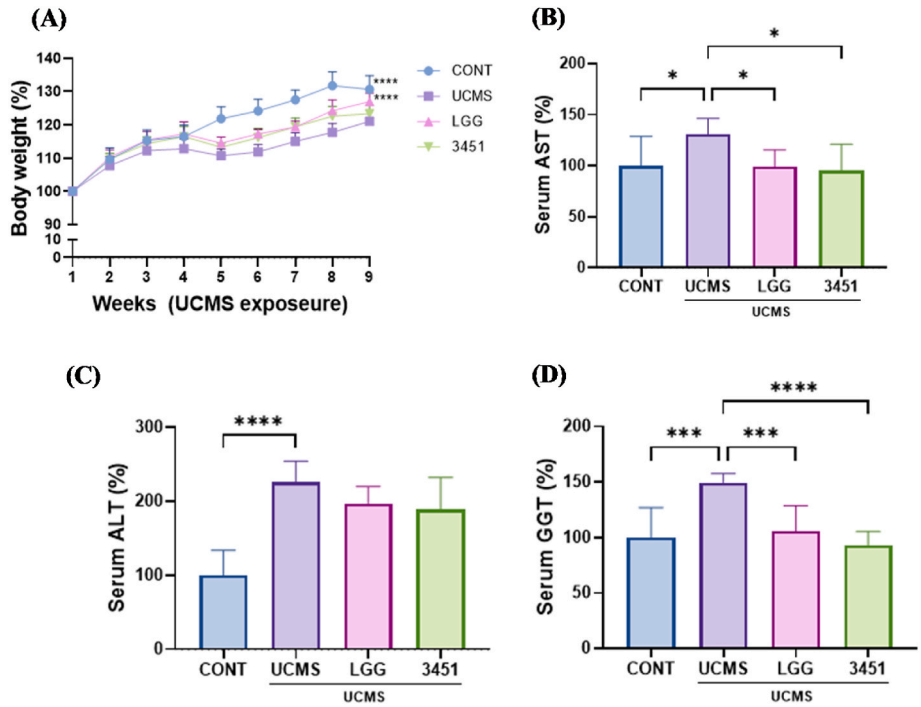

Fig. 5. (A) Body weight change of the mice weekly, serum (B) AST, (C) ALT concentration, and (D) GGT in the UCMS study. Results are expressed as mean ± standard error mean (SEM); $n = 8$ per group. *Means in the same series with significantly different (*, $p < 0.05$; **, $p < 0.01$; ***, $p < 0.001$; ****, $p < 0.0001$).

These microbial and metabolic changes appeared interrelated. Notably, *Coprococcus*, *Akkermansia*, and *Ruminococcus* showed strong positive correlations with elevated levels of glycine, L-leucine, L-glutamic acid, and glycerol levels in the 3451 group (Fig. 7L). Moreover, compositional changes in phyla such as Firmicutes, Proteobacteria, Bacteroidetes, Tenericutes, Deferribacteres, Actinobacteria, Verrucomicrobia, and unclassified bacteria were associated with alterations in amino acids, organic acids, fatty acids, lipids, alcohols, and phenolic compounds (Fig. 7B). These findings suggest that 3451 modulates gut microbial composition and metabolite production in a coordinated manner, potentially contributing to its therapeutic effects in UCMS-induced behavioral and physiological impairments.

2.7. Body weight and serum biochemical analysis in the DSS model

To evaluate the health and nutritional status of the mice, body weight, feed intake, and water intake were measured. There were no significant differences between groups in daily feed and water intake (Fig. 8A, Suppl 3A–B). After 7 days of exposure to the DSS, the body weight ratios relative to initial weight were 104.4 %, 85.4 %, 88.5 %, and 87.1 % in the CONT, DSS, LGG, and 3451 groups, respectively. While body weight was slightly higher in the LGG and 3451 groups than in the DSS group, the differences were not statistically significant (Fig. 8A). The disease activity index (DAI) was assessed to monitor disease progression, symptom severity, and treatment efficacy in DSS-induced colitis. DAI is a composite clinical score that integrates three major indicators of colitis severity: body weight loss, stool consistency, and rectal bleeding. A higher DAI score reflects a more pronounced disturbance in intestinal function and greater inflammation-induced pathology. Compared to the DSS group, the CONT, LGG, and 3451 groups exhibited lower DAI scores throughout the experimental period (Fig. 8B). Notably, on day 7, both the CONT and 3451 groups showed significantly reduced DAI scores ($p < 0.0001$ and $p = 0.0358$, respectively), indicating substantial mitigation of DSS-induced clinical symptoms. These results highlight the therapeutic effect of 3451 in alleviating intestinal inflammation and improving clinical outcomes in the colitis model.

In serum biochemical analysis, AST levels were significantly lower in the CONT, LGG, and 3451 groups than in the DSS group ($p = 0.0123$, $p = 0.0233$, and $p = 0.0123$, respectively; Fig. 8C). Although ALT levels did not differ significantly, both LGG and 3451 groups showed downward trends compared to the DSS group, with ALT ratios of 70.7 % and 62.1 %, respectively, versus 106.9 % in the DSS group (Fig. 8D). Regarding inflammatory cytokines, IL-6 levels were significantly reduced in the CONT, LGG, and 3451 groups relative to the DSS group ($p = 0.0002$, $p = 0.0018$, and $p = 0.0204$, respectively) (Fig. 8E). Meanwhile, the anti-inflammatory cytokine IL-10 showed significantly higher levels in the CONT and 3451 groups than in the DSS group ($p = 0.0161$ and $p = 0.0017$, respectively) (Fig. 8F).

2.8. Colon morphologic and qPCR analysis

To evaluate DSS-induced structural damage in the colon, hematoxylin and eosin (H&E) and periodic acid–Schiff (PAS) staining were performed (Fig. 9A). Histological scoring revealed significantly reduced tissue damage in the CONT, LGG, and 3451 groups compared to the DSS group ($p < 0.0001$, $p = 0.0002$, and $p = 0.0002$, respectively) (Fig. 9B). Goblet cell preservation, as measured by Goblet cell/crypt ratio, was significantly higher in the CONT, LGG, and 3451 groups relative to the DSS group ($p < 0.0001$ for all comparisons) (Fig. 9C), indicating restoration of mucosal integrity. Colon length was markedly shortened in all DSS-exposed groups (DSS, LGG, and 3451) compared to the unchallenged CONT group ($p < 0.0001$) (Fig. 9D), confirming the severity of DSS-induced colitis.

qPCR analysis further supported the protective effects of 3451. Gene expression of the tight junction protein *ZO-1* was significantly upregulated in the 3451 group compared to the DSS group ($p = 0.0133$) (Fig. 9E). *Claudin1* expression was significantly increased in the LGG group ($p = 0.0416$), while the 3451 group showed a nonsignificant upward trend compared to DSS (mean values: 1.594 vs. 1.049) (Fig. 9F). *Occludin* expression was lowest in the DSS group and modestly elevated in the CONT, LGG, and 3451 groups, although no significant differences were observed (Fig. 9G).

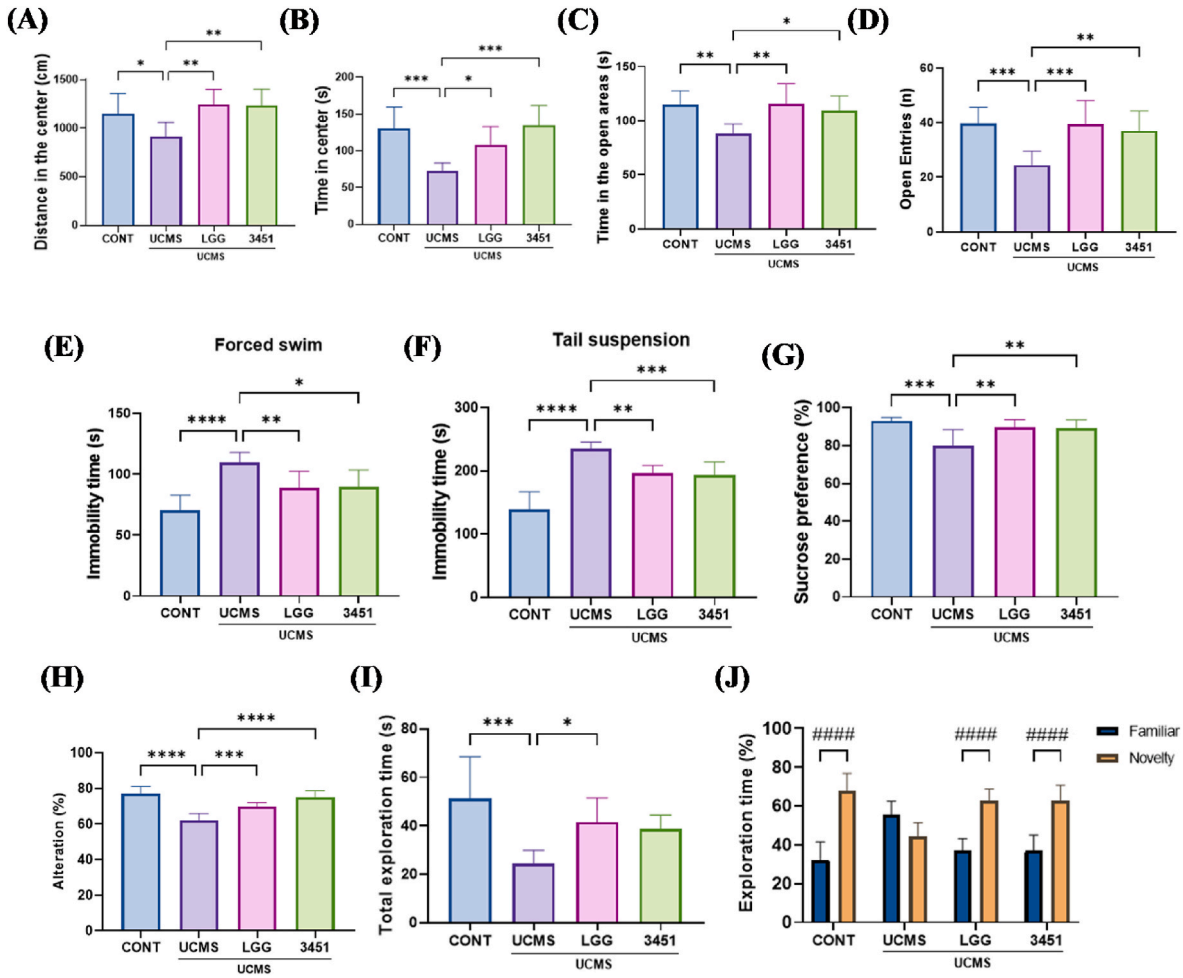

Fig. 6. Effect of the *Lacticaseibacillus casei* IDCC 3451 on the results of the behavior test. (A–B) OFT, (C–D) EZM, (E) total immobility time in FST, (F) TST, (G) sucrose preference (H) Y-maze, (I–J) NOR, and colon mRNA expression level of (K) ZO-1, (L) claudin1, and (M) occludin in the UCMS mouse model. Results are expressed as mean ± standard error mean (SEM); $n = 8$ per group. *Means in the same series with significantly different (*, $p < 0.05$; **, $p < 0.01$; ***, $p < 0.001$; ****, $p < 0.0001$).

2.9. Correlation analysis for metagenome and metabolome in the DSS model

To assess the interplay between gut microbial composition and metabolite profiles, a correlation analysis was conducted in the DSS-induced colitis model following 3451 administration. Treatment with 3451 significantly increased the relative abundance of *Coprococcus*, *Butyricimonas*, *Bifidobacterium*, *Parabacteroides*, and *S24-7* compared to the DSS group (Fig. 10A).

Metabolomic analysis revealed significantly elevated levels of L-threonine, L-threonic acid, propionic acid, L-glutamic acid, valeric acid, and inositol in the 3451 group (Fig. 10C–K). In addition, amino acids such as L-tryptophan, L-phenylalanine, and L-serine showed increasing trends. These shifts suggest that changes in the gut microbiota induced by 3451 are accompanied by increased production of amino acids and short-chain fatty acids.

Notably, *Coprococcus*, *Butyricimonas*, and *Bifidobacterium* displayed strong correlations with significantly increased levels of L-threonine, L-threonic acid, propionic acid, L-glutamic acid, and inositol in the 3451 group compared to the DSS group (Fig. 10L), supporting a link between bacterial taxa and specific metabolic outputs. At the phylum level, changes in Firmicutes, Bacteroidetes, Actinobacteria, Proteobacteria, Cyanobacteria, Verrucomicrobia, unclassified Bacteria, and Tenericutes were associated with corresponding alterations in amino acids, organic acids, fatty acids, and phenolic compounds (Fig. 10B). These findings suggest that 3451 modulates gut microbial and metabolic networks in a coordinated fashion, contributing to the alleviation of colitis-related dysbiosis.

3. Discussion

This study first evaluated the biological effects of *Lacticaseibacillus casei* IDCC 3451 (3451) using the *C. elegans* model, a genetically tractable organism widely employed for studies on host–microbe interactions, aging, and neurodegeneration due to its short lifespan and transparent anatomy (Tissenbaum, 2015). Treatment with 3451 led to a significant extension of lifespan compared to the standard *E. coli* OP50 diet, consistent with prior research demonstrating the longevity-promoting effects of probiotics (Choi et al., 2023; Park et al., 2018; Zhou et al., 2021). Killing assays further revealed that 3451 enhanced host defense against both Gram-negative (*E. coli* O157:H7 EDL933) and Gram-positive (*S. aureus* Newman) pathogens, underscoring its role in strengthening innate immunity (Ryu et al., 2019; Kim et al., 2022). These effects are in line with previous studies on *Lactobacillus* strains showing activation of host immune responses (Park et al., 2018; Huang et al., 2024b; Dong et al., 2025).

Beyond survival, 3451 significantly improved neuromuscular and behavioral function in *C. elegans* strains expressing human amyloid beta, a hallmark of neurodegeneration. Specifically, 3451 treated worms exhibited enhanced thrashing frequency, improved chemotaxis toward

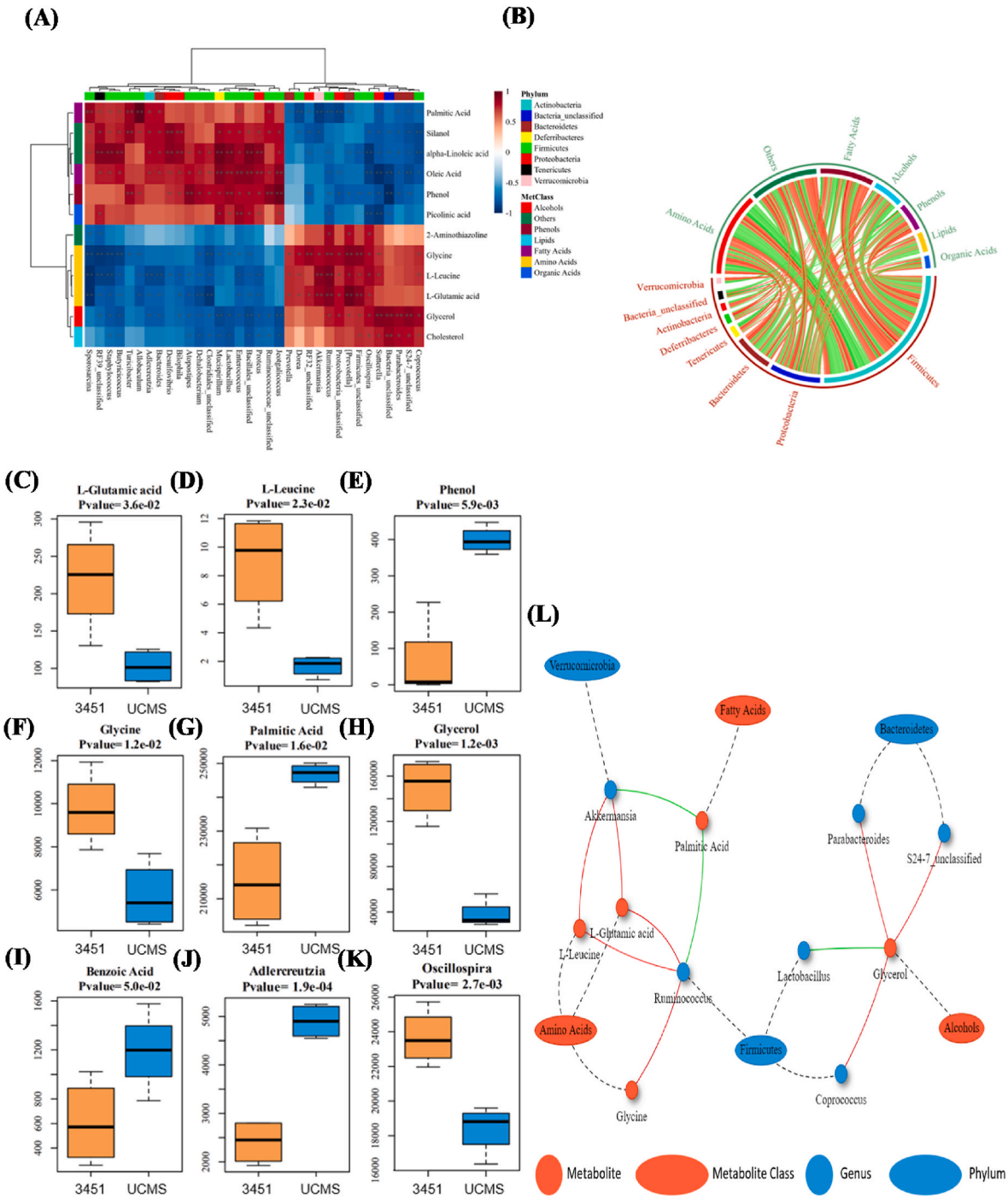

Fig. 7. Effect of *Lacticaseibacillus casei* IDCC 3451 on the correlation between fecal microbiota and metabolites. (A) The heatmap displays Spearman correlation coefficients between differentially abundant microbial genera and metabolites. Asterisks indicate statistically significant correlations: (*, $p < 0.05$; **, $p < 0.01$. (B) Circos plot, and (C–K) boxplots represent metabolites that differ between UCMS and 3451 groups. (L) Network shows the Spearman correlation between microbiota and metabolites of the 3451 group; mean (SD) values of each group are provided by the Student's t-test.

attractants, and increased pharyngeal pumping rates, all of which indicate restoration of sensory-motor coordination and feeding behavior. These findings are consistent with previous reports demonstrating that probiotic strains, including *Lactobacillus paracasei* and lactic acid bacteria, can mitigate amyloid beta toxicity and restore locomotor behavior in transgenic *C. elegans* models (Kumaree et al., 2023; Urrutia et al., 2020). Imaging analysis revealed a marked reduction in GFP-labeled amyloid beta aggregates in the 3451 group, suggesting a direct neuroprotective effect. This observation aligns with prior studies showing that probiotics or bacterially derived metabolites can suppress protein aggregation and neuronal degeneration in *C. elegans* (Goya et al., 2020; Goyache et al., 2024; Wu and Luo, 2005).

At the molecular level, transcriptomic and gene network analysis revealed upregulation of several protective gene classes. Anti-aging responses were activated via increased expression of *daf-16/FOXO*, while immune-related genes such as *CaeNaCin* and *C-type lectin* families were induced. 3451 also upregulated genes related to neurotransmission and downregulated serine/threonine phosphatase-associated genes.

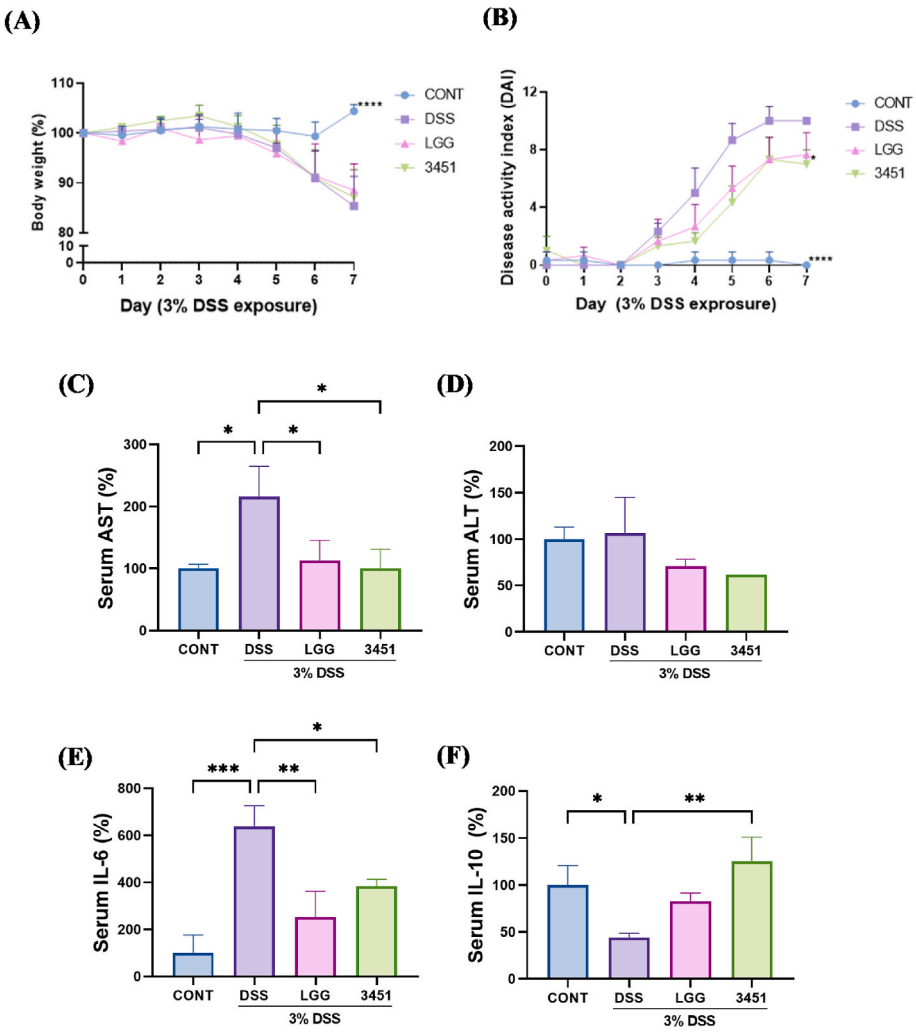

Fig. 8. Effect of *Lacticaseibacillus casei* IDCC 3451 on colitis mouse (A) body weight, (B) DAI, and serum levels of (C) AST, (D) ALT, (E) IL-6, and (F) IL-10 in the DSS-induced colitis model. CONT, normal control group; DSS, DSS-only treated group; LGG, positive control group; 3451, 3451 strain-treated group. [1]Results are expressed as the mean; $n = 3$ per group. *Means in the same series with significantly different (*, $p < 0.05$; **, $p < 0.01$; ***, $p < 0.001$; ****, $p < 0.0001$).

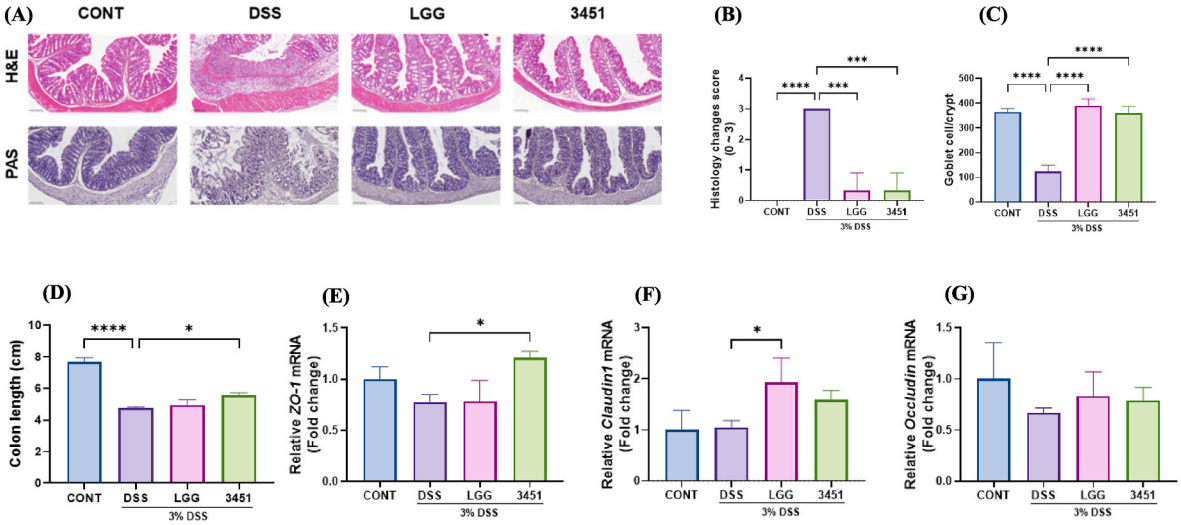

Fig. 9. Effect of *Lacticaseibacillus casei* IDCC 3451 the intestinal barrier integrity on mouse (A) colon morphology, (B) histological score, (C) goblet cell count, (D) colon length, and colon mRNA expression level of (E) ZO-1, (F) claudin1, and (G) occludin in the DSS-induced colitis model. CONT, normal control group; DSS, DSS-only treated group; LGG, positive control group; 3451, 3451 strain-treated group. [1]Results are expressed as the mean; $n = 3$ per group. *Means in the same series with significantly different (*, $p < 0.05$; **, $p < 0.01$; ***, $p < 0.001$; ****, $p < 0.0001$).

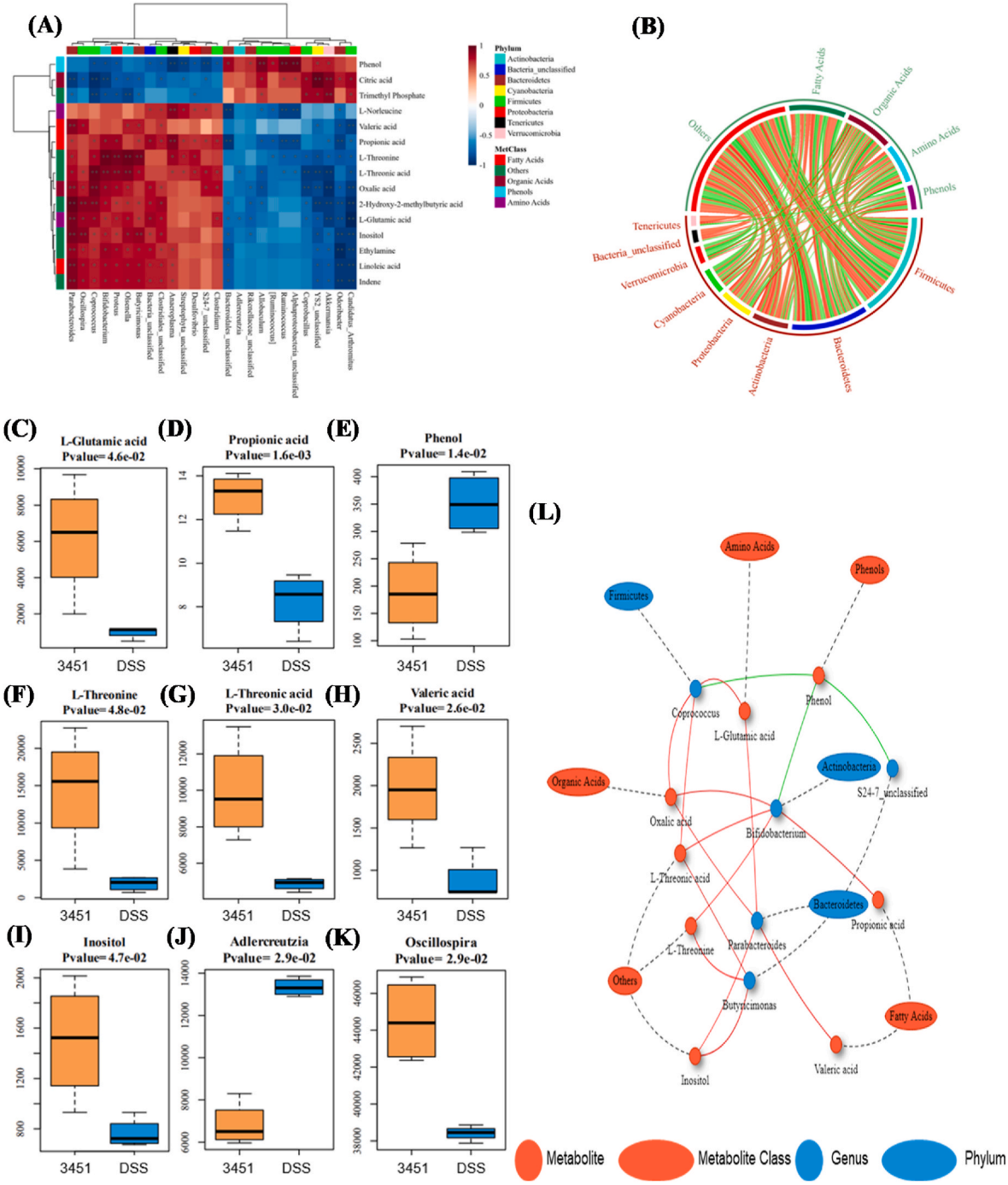

Fig. 10. Correlation analysis between gut microbiota and its metabolites produced after administration of *Lacticaseibacillus casei* IDCC 3451 in the DSS-induced colitis model. (A) The heatmap displays Spearman correlation coefficients between differentially abundant microbial genera and metabolites in the 3451 group. Asterisks indicate statistically significant correlations: (*, $p < 0.05$; **, $p < 0.01$. **(B)** Circos plot of Spearman correlations between microbiota and metabolites (green, positive correlation; red, negative correlation). **(C–K)** Boxplots of different levels of metabolites between DSS and 3451; mean (SD) values of each group are provided by the Student's t-test. **(L)** Visualized network Spearman correlation. DSS, DSS-only treated group; 3451, 3451 strain-treated group.

Additionally, increased expression of *spi-1*, encoding a serine protease inhibitor, suggests improved proteostasis and neuroimmune signaling. Together, these results suggest that 3451 exerts a multifaceted neuroprotective effect by restoring host gene networks implicated in longevity, immunity, and nervous system function.

In conclusion, these findings collectively highlight the potential of *L. casei* IDCC 3451 as a multifunctional probiotic in the *C. elegans* model. 3451 not only extended lifespan and enhanced innate immunity but also ameliorated behavioral deficits associated with amyloid beta toxicity and modulated gene networks related to anti-aging and neuronal function. These results provide mechanistic insight into its neuroprotective properties and open new avenues for exploring the translational relevance of 3451 in higher organisms. Further investigations are warranted to elucidate its therapeutic potential and applicability in complex disease models.

Chronic psychological stress is known to induce a wide spectrum of physiological and behavioral disturbances, including anxiety, depression, cognitive decline, and metabolic imbalance (Lupien et al., 2018;

Kendler et al., 2011). These effects are mediated through neuroendocrine disruption, immune dysregulation, and alterations in gut microbiota composition. The microbiome–gut–brain axis has thus emerged as a critical therapeutic target, with psychobiotics such as *L. casei* IDCC 3451 gaining attention for their regulatory potential (Vanderhoof, 2001).

In this study, the unpredictable chronic mild stress (UCMS) model was employed to assess the efficacy of 3451 in mitigating stress-induced dysfunctions. To evaluate behavioral outcomes associated with stress-induced dysfunction, we employed a series of well-established paradigms for assessing locomotor activity, anxiety-like behavior, and depressive-like states, respectively, in murine models. These tests have been extensively applied in neuroinflammation and stress-related studies, particularly in the context of gut–brain axis research, due to their sensitivity to both central nervous system modulation and peripheral immune influences (Bonaz et al., 2018; Gould et al., 2009; Kraeuter et al., 2019; Lueptow, 2017). UCMS-exposed mice exhibited decreased weight gain and significant behavioral impairments related to anxiety, depression, and cognition; findings consistent with prior studies on stress-induced neuropathology (Lupien et al., 2018; Hu et al., 2014). Oral administration of 3451 ameliorated these deficits, as shown by increased exploratory behavior in the open field and elevated zero maze tests, along with reduced immobility in the forced swim and tail suspension tests.

At the molecular level, 3451 restored the expression of 5HT1AR and GABA receptors, indicating modulation of serotonergic and GABAergic signaling. Importantly, the expression of aromatic L-amino acid decarboxylase (AADC) in the colon was upregulated, suggesting enhanced peripheral serotonin synthesis and reinforcement of gut-brain communication (Shajib et al., 2017). Additionally, 3451 downregulated *Cyp11b1*, reducing corticosterone overproduction and associated neurotoxicity. *BDNF* expression was also restored, accompanied by a rebalancing of proapoptotic and antiapoptotic gene expression. UCMS disrupted the expression of tight junction proteins such as *ZO-1*, reflecting compromised gut barrier function (van de Wouw et al., 2018; Wang et al., 2008). 3451 effectively reversed these changes, supporting its role in maintaining epithelial integrity.

Metagenomic analysis further revealed that 3451 restored the abundance of commensal microbial families including *Lachnospiraceae* and *Ruminococcaceae*, which are known producers of short-chain fatty acids (SCFAs) such as butyrate. These metabolites play a key role in maintaining intestinal barrier integrity and regulating inflammation, suggesting that 3451 contributes to the re-establishment of a healthy and functionally beneficial microbial ecosystem (Cryan et al., 2019; Fung et al., 2017). Although alpha diversity remained relatively unchanged, significant shifts in beta diversity indicated compositional reorganization of the microbiota toward a more homeostatic profile. These findings underscore the ability of 3451 to counteract the behavioral, molecular, endocrine, and microbiological disruptions induced by chronic stress, and highlight its potential as a psychobiotic intervention for neuropsychiatric disorders.

In the DSS-induced colitis model, oral administration of *L. casei* IDCC 3451 markedly alleviated core clinical symptoms, including weight loss, diarrhea, and histological damage to the colonic mucosa. Histopathological analysis demonstrated improved epithelial structure and reduced crypt distortion and inflammatory infiltration. These effects are consistent with previous findings showing that multispecies synbiotics or probiotic strains can protect intestinal tissue integrity and suppress inflammation in DSS-challenged mice (Wang et al., 2020; Xia et al., 2020).

On the molecular level, 3451 restored the expression of tight junction proteins, such as *ZO-1* and *Claudin1*, indicative of enhanced epithelial barrier integrity. This restoration was accompanied by upregulation of the anti-inflammatory cytokine IL-10 and suppression of IL-6, a key mediator of mucosal inflammation (Cai et al., 2024; Yu et al., 2020). Microbiota profiling revealed that 3451 reversed DSS-induced dysbiosis, increasing the relative abundance of beneficial commensals such as *Lachnospiraceae*, *Ruminococcaceae*, and *Bacteroidetes*, which are often depleted in IBD patients (Wang et al., 2020; Xia et al., 2020; Yu et al., 2020). Furthermore, metabolomic analysis showed elevated levels of SCFAs, including butyrate and propionate, metabolites known to support intestinal epithelial repair and immunoregulation. These changes were positively correlated with increases in SCFA-producing genera such as *Coprococcus*, *Butyricimonas*, and *Bifidobacterium*, underscoring a functional interaction between microbial community shifts and host metabolic outcomes.

Collectively, these results demonstrate that 3451 attenuates intestinal inflammation, strengthens mucosal barrier integrity, and reestablishes gut microbial and metabolic homeostasis in the DSS-induced colitis model. These findings highlight the therapeutic potential of 3451 for inflammatory bowel disease through integrated modulation of host–microbe interactions.

4. Conclusion

Our findings demonstrate that *L. casei* IDCC 3451 confers multisystemic benefits through coordinated modulation of the gut-brain axis. These effects span enhanced longevity, neuromuscular function, and behavioral performance; restoration of neurotransmitter signaling and neurotrophic support; preservation of intestinal barrier integrity; and normalization of gut microbiota and host metabolite profiles.

However, it is important to acknowledge several limitations. While both *C. elegans* and murine models provide valuable mechanistic insight, they cannot fully replicate the complexity of human gastrointestinal and neurological systems. The duration of probiotic administration was limited to several weeks, which may not be sufficient to capture long-term physiological or behavioral changes. Although our data identified several candidate pathways and microbial taxa potentially associated with the observed effects, we did not perform direct mechanistic validation using gene knockouts or receptor-specific interventions. Therefore, future studies that incorporate long-term treatment protocols, pathway-specific modulation, and clinical cohorts are crucial to confirm the relevance of our findings.

Despite the acknowledged limitations, our findings suggest the potential of *L. casei* IDCC 3451 as a psychobiotic candidate. This strain shows promise in modulating microbiota-driven neuroimmune pathways, indicating its potential therapeutic role in managing neuroinflammatory and gastrointestinal disorders. However, further research, including long-term studies, mechanistic dissection, and clinical translation, is necessary to confirm its applicability.

5. Methods

5.1. Bacterial strains and culture conditions

Lacticaseibacillus casei IDCC 3451 (3451) and *Lacticaseibacillus rhamnosus* GG (LGG) were cultivated at 37 °C for 48 h in MRS broth (BD Biosciences). The 3451 strain was provided by Ildong Bioscience (Seoul, South Korea) and selected based on prior evidence of its immunomodulatory and neuroprotective properties (Shin et al., 2021). LGG was used as a positive control, given its well-established efficacy as a model psychobiotic strain with documented effects on gut-brain communication and barrier function (Liu et al., 2022; Zhou et al., 2022). *E. coli* OP50, the standard food source for *C. elegans*, was used as a baseline dietary control (Kim et al., 2021; McIntyre et al., 2021). In addition, *Escherichia coli* O157:H7 EDL933 and *Staphylococcus aureus* Newman were selected as representative Gram-negative and Gram-positive pathogens, respectively, for evaluating host immune responses under pathogenic challenge (Kim et al., 2021; Zeng et al., 2024). These strains were cultured in Luria-Bertani broth (*E. coli* OP50, *E. coli* EDL933) or brain heart infusion broth (*S. aureus*) at 37 °C for 24 h.

To prepare live bacterial lawns for feeding to *C. elegans*, a bacterial

pellet was collected by centrifugation at 6000 rpm for 10 min, washed twice with sterile M9 buffer (3 g KH_2PO_4, 5 g NaCl, and 6 g Na_2HPO_4), and dissolved in 1 L distilled H_2O. After autoclaving, 1 mL of 1 M $MgSO_4$ was added. Subsequently, the purified bacterial pellet was suspended in M9 buffer, seeded on NGM plates, and dried.

5.2. C. elegans strains and culture conditions

C. elegans were maintained on NGM agar at 15 °C using standard techniques (Brenner, 1974). Eggs of *C. elegans* were collected using a sodium hypochlorite–sodium hydroxide solution, and synchronized L1 worms were grown to the young adult L4 stage at 25 °C on NGM plates seeded with *E. coli* OP50. *C. elegans* mutant strains, including CF512 (fer-15(b26)II; fem-1(hc17)IV), CL2120(dvIs14 [(pCL12) unc-54Aβ 1–42 + (pCL26) mtl-2green fluorescent protein (GFP)]), CL2122(dvIs15 [(pPD30.38) unc-54 (vector) + (pCL26) mtl-2GFP]), and CL4176(dvIs27 X [myo-3pAβ (1–42)let-851 3′UTR] + rol-6(X), were used. CF512, which could not produce progeny at 25 °C without phenotypic differences, was used for transcriptome analysis, lifespan, and killing assays. CL2120 and CL4176 mutant strains from an AD model were treated with different bacterial strains, and thrashing, pharyngeal pumping, and chemotaxis were monitored. CL2122 was used as a control strain for CL2120 and CL4176.

5.3. C. elegans lifespan and killing assays

For the lifespan assay, young adult L4 stage CF512 worms were transferred, using a platinum wire, onto a 35-mm-diameter NGM plate seeded with 100 μL of concentrated 3451, *E. coli* OP50, or LGG. For the killing assay, young adult L4 stage CF512 worms were placed on a 60-mm-diameter NGM plate seeded with 200 μL of concentrated 3451, *E. coli* OP50, or LGG for 48 h. Subsequently, worms were transferred to a 35-mm NGM plate seeded with pathogenic bacteria, *S. aureus* Newman or *E. coli* O157:H7 EDL933, using a platinum wire. *E. coli* OP50 and LGG were used as normal controls and positive controls, respectively. Worms were incubated at 25 °C, and a total of 90 worms were used for each bacterial species in three separate plates. Live worms were counted every day and transferred to a fresh NGM plate seeded with each bacterial strain once every 2 days until no live worms were observed.

5.4. C. elegans behavior assays

In behavioral assays in *C. elegans*, thrashing, pharyngeal pumping, and chemotaxis were assessed using corresponding behavioral assays on days 0 and 5 of life. In assays, an amyloid beta accumulation genetic mutant strain, CL4176, and a control strain of CL4176, CL2122, were used. For the thrashing assay, the number of thrashings in the M9 buffer was observed to assess the motility of the worms. Individual worms (n = 10 per group) were transferred to bacteria-free, sterile 35-mm-diameter NGM agar plates and allowed to crawl for 1 min to remove aggregated bacteria. Subsequently, 20 μL of M9 buffer was dropped on the worm, allowing the worm to adapt for 1 min, and the number of thrashings was counted for 30 s. To measure the pharyngeal pumping of *C. elegans*, the worms (n = 10 per group) were then transferred to a new *E. coli* OP50 or potential probiotic-seeded 35-mm-diameter NGM agar plates. Subsequently, the pharyngeal region of the worm was video recorded, and the video was analyzed to count the number of pharyngeal muscle pumps the worm pumped in 30 s. Chemotaxis refers to the migration of *C. elegans* toward attractants or away from repellents. To assess the chemotaxis behavior of *C. elegans*, the degree of response of the worms to the attractant and repellent chemicals was measured. 3451- or *E. coli* OP50-exposed 50–250 worms were moved to a sterile 60-mm-diameter NGM plate without bacteria and allowed to crawl for a minute to remove the aggregated bacteria (n = 6 per group). Another sterile 60-mm-diameter NGM agar plate was prepared with a drop of 100 mM isoamyl alcohol diluted in 100 % EtOH as an attractant, dried at 2 cm from the center circle. Subsequently, 100 % EtOH was prepared as a control in the same way as the attractant. After moving the worms to the center circle of the plate and allowing them to crawl freely, after 1 h, the number of worms located in each control or attractant area was measured. The same method was repeated with the repellent, 30 % octanol (v/v) in 100 % EtOH.

5.5. C. elegans GFP fluorescence analysis

To measure the area of GFP fluorescence expression in *C. elegans*, CL2120 and CL2122 strains exposed for 5 days to 60-mm NGM plates seeded with 3451 or *E. coli* OP50 were used (n = 5 per group). Day 5 worms were centrifuged at 3500 rpm for 1 min, and the supernatant was removed. Subsequently, 10 μL of *C. elegans* suspension was placed on a glass slide with 2 % agarose gel and covered with a coverslip. *C. elegans* was imaged using an Olympus IX53 microscope (Olympus, Tokyo, Japan). The GFP fluorescence expression area of the worm was analyzed using ImageJ software. The GFP fluorescence expression area data are expressed as Aβ deposits/total worm area (Wang et al., 2022).

5.6. C. elegans transcriptomic analysis

Young adult L4 stage CF512 worms were placed on a 60-mm-diameter NGM plate seeded with 200 μL of concentrated 3451 or *E. coli* OP50 for 48 h. Total RNA was extracted using TRIzol reagent (Invitrogen, Carlsbad, CA, USA) and purified using the RNeasy Mini Kit (QIAGEN, Valencia, CA, USA) according to the manufacturer's instructions. Quality and quantity checks, RNA sequencing, and transcriptome analysis of the isolated total RNA sample were performed by Macrogen (Macrogen Inc., South Korea). To analyze the function of differentially expressed genes, the Cluego plug-in in Cytoscape software (3.9.1 version) was used.

5.7. UCMS-induced behavioral impairment mouse model

To establish a UCMS-induced behavioral impairment mouse model, C57BL/6 male mice (aged 4 weeks) were obtained from Central Lab. Animal Inc. (Seoul, South Korea). Subsequently, five mice per cage were housed and maintained at 22 °C ± 2 °C with 50 % ± 10 % humidity and subjected to a 12-h light/dark cycle. To minimize environmental and dietary confounding factors, all animals were maintained under identical housing conditions with standardized chow and water, and experimental groups were housed in the same room throughout the study.

All mice were acclimatized for a week to the normal diet. After weighing, the mice were randomly divided into four groups (n = 15 per group): CONT, vehicle control group, mice administered orally with saline (100 μL/day); UCMS, negative control group, stressed mice administered orally with saline (100 μL/day); UCMS + LGG (LGG), positive control group, stressed mice administered orally with LGG (1×10^8 CFU/day); and UCMS + 3451 (3451), probiotic treatment group, stressed mice administered orally with 3451 (1×10^8 CFU/day) (Fig. 4A). During the experiment, all groups received oral administration for 10 weeks. The UCMS, LGG, and 3451 groups were exposed to unpredictable chronic stress from the 3rd to the 10th week, and all groups underwent behavioral tests from the 6th to the 10th week. The UCMS groups (UCMS, LGG, and 3451) were exposed in random order to different and unpredictable chronic stressors, such as illumination, food deprivation, water deprivation, cold objects, tail tie-up, restraint, water bath, empty cage, wet cage, tilted cage, and foreign cage. All animal experimental protocols were conducted according to the procedures and permits approved by the Institutional Animal Care and Use Committee of Sejong University (certificate SJ-20230110-01). To establish the DSS-induced colitis mouse model, C57BL/6 male mice (aged 7 weeks) were obtained from SamTako Bio (Korea) (Fig. 4B). Subsequently, five mice per cage were housed and maintained at 23 °C ± 1 °C with 55 % ± 5 %

humidity and subjected to a 12-h light/dark cycle. All mice were acclimatized for a week to the normal diet. After weighing, the mice were randomly divided into four groups ($n = 6$ per group): CONT, vehicle control group, mice administered orally with PBS (200 μL/day) and receiving autoclaved tap water; DSS, negative control group, mice administered orally with PBS (200 μL/day) and receiving 3 % DSS solution; DSS + LGG (LGG), positive control group, mice administered orally with LGG (1×10^9 CFU/day) and receiving 3 % DSS solution; and DSS + 3451 (3451) probiotic treatment group, mice administered orally with 3451 (1×10^9 CFU/day) and receiving 3 % DSS solution. During the experiment, all groups received oral administration for 14 days, and DSS, LGG, and 3451 groups received DSS from day 7 (DSS 0). From days 7 (DSS 0) to 14 (DSS 7), food intake, water intake, and body weight were measured every day. All animal experimental protocols were conducted according to the procedures and permits approved by the Institutional Animal Care and Use Committee of Seoul National University (certificate SNU-221025-2).

5.8. Open-field test

The open-field test (OFT) is used to measure anxiety-like behavior in animals (Belovicova et al., 2017). The OFT apparatus consisted of an empty square arena (40 × 40 × 30 cm) with 30-cm walls. The experiment started immediately after the mouse was placed in the corner of the open-field chamber and monitored for 20 min. The total distance traveled by the mouse represents basic locomotor activity. Time spent by mice in the corner zone indicates anxiety-like behavior.

5.9. Elevated zero maze test

The elevated zero maze (EZM) test is used to measure anxiety-like behavior in animals (Belovicova et al., 2017). The EZM consisted of a circular apparatus with a diameter of 60 cm, enabling the mice to travel a 10-cm-wide path. The EZM consisted of two open areas and two closed areas. The walls of the closed area were 31 cm high. The test was conducted at a height of 62 cm from the ground. Each mouse was placed in the closed area of the maze, and the experiment commenced, lasting for 5 min. By observing the mice's exploration patterns during this time, this study aimed to evaluate their anxiety levels and propensity for open-area exploration.

5.10. Forced swimming test

The forced swimming test (FST) is used to measure depression-like behavior in animals (Belovicova et al., 2017). The FST apparatus consisted of a 5-L glass beaker (19 Ø × 26 cm). The beaker was filled with water and maintained at a temperature of 25 °C ± 1 °C, reaching a depth of 16 cm. The test duration was set at 6 min, during which the immobility time of the mice was measured for a period of 4 min, starting 2 min after the test initiation.

5.11. Tail suspension test

The tail suspension test (TST) is used to measure depression-like behavior in animals (Belovicova et al., 2017). The TST apparatus had dimensions of 15 cm in width, 10 cm in length, and 50 cm in height. A stick was placed horizontally over the apparatus to facilitate the test. During the experiment, the tail of each mouse was gently taped to the stick, allowing the mouse to hang freely. The test duration was set at 6 min, during which the behavior of the mouse was observed.

5.12. Sucrose preference test

The sucrose preference test (SPT) is used to measure depression-like behavior in animals (Belovicova et al., 2017). Before the experiment, a sucrose habituation phase and a liquid tube habituation phase were conducted over 62 h. The test was performed in a chamber (11 × 23 × 12). During the test phase, the mice were given access to two liquid tubes: one containing 1 % sucrose water and the other containing regular water. The mice were allowed to freely explore and consume from the tubes for a duration of 12 h. The weights of the liquid tubes were measured before and after the test to calculate the consumption amount.

5.13. Spontaneous alternation Y-maze test

The Y-maze (Y-maze) test is used to measure short-term memory in animals (Kraeuter et al., 2019). The Y-maze apparatus consisted of three arms, each measuring 36 cm in length and 16 cm in height. The experiment had a duration of 8 min, and each mouse was placed in the center of the maze to commence the test.

5.14. Novel object recognition test

The novel object recognition (NOR) test is used to measure learning and memory in animals (Lueptow, 2017). The NOR apparatus used had dimensions of 40 cm in width, 40 cm in length, and 40 cm in height. The NOR test consisted of two phases: the training phase and the test phase. During the training phase, two similar familiar objects (a triangle and a square) were placed in the apparatus. Following a 24-h interval, the test phase commenced. In this phase, one of the familiar objects was randomly replaced with a novel object (a circle). The mouse was then placed in one of the corners of the apparatus, and the experiment commenced for a duration of 5 min. For all behavioral tests, the apparatus was wiped with 70 % ethanol and completely dried after experimenting with one animal, and the next mouse experiment was started.

5.15. Evaluation of the disease activity index

The Disease Activity index (DAI) score evaluates the severity of UC. The DAI score was measured with reference to previous studies (Huang et al., 2022; Chen et al., 2007). The DAI score includes weight loss (0, no weight loss; 1, 1 %–5 %; 2, 5 %–10 %; 3, 10 %–15 %; 4, >20 %), stool consistency (0, normal; 1, loose stools; 2, mild diarrhea; 3, diarrhea; 4, watery diarrhea), and hematochezia (0, no bleeding (negative); 1, trace bleeding; 2, slight bleeding; 3, obvious bleeding; 4, gross bleeding). The hematochezia score was determined using the Hema-Screen Lab Pack for fecal occult blood (EKF Diagnostics, Boerne, TX, USA).

5.16. Colon length measurement

After sacrificing, colon samples were washed with PBS and collected from the cecum to the rectum. The colon tissue of mice for each group was pictured with a ruler. The length of the colon was measured using ImageJ software version 1.8.0 (W. Rasband, USA).

5.17. Hematoxylin and eosin staining

Colon samples from each mouse were washed with sterile PBS. Samples were fixed in 10 % formalin, washed, and subjected to dehydration and clearing in an automated tissue processor (Nussloch, Germany, Automatic Tissue Processor, Leica). After embedding the sample in a paraffin block (Nussloch, Germany, Embedding Center, LEICA, EG1150H), it was cut into 4–6 μm using a cutting machine (LEICA, RM2135) to prepare a slide. Samples were stained with hematoxylin and eosin (H&E) staining reagents and analyzed by imaging with a kfbio digital slide scanning system (Konfoong Bioinformation Tech Co., Ltd.). A histological score evaluates the severity of inflammation, cell damage, and tissue architecture, and the score was scored from 0 to 3 according to the degree of histopathologic change (0, negative, no meaningful histopathologic change; 1, positive, mild degree; 2, positive, moderate degree; 3, positive, severe degree).

5.18. Periodic acid–Schiff staining

Samples of the colon from the mouse were stained with Periodic Acid–Shiff (PAS) staining reagents. The process of sample fixation, embedding, imaging, analysis, and slide preparation is the same as H&E staining. The stained samples are then examined under a microscope, and the number of goblet cells in each crypt is counted and recorded. The score is calculated as the average number of goblet cells per crypt in a given area of tissue.

5.19. Serum biochemical analysis

Blood samples were collected from the postcaval veins of mice, centrifuged at 1500×*g* for 15 min to obtain serum, and stored at −80 °C for further analysis. Aspartate transaminase (AST/GOT) and alanine transaminase (ALT/GPT) were measured using Embiel glutamate oxaloacetate transaminase (GOT), glutamate pyruvate transaminase (GPT), and gamma-glutamyl transpeptidase (GGT) test kits (Embiel Ltd., Korea) to confirm the degree of inflammation in the mice. The levels of IL-6 (Abcam, 222503) and IL-10 (Abcam, ab255729) were measured using enzyme-linked immunosorbent assay kits.

5.20. RNA isolation and RT-qPCR analysis

Total RNA was extracted using the RNeasy Plus kit (Qiagen, Hilden, Germany) according to the manufacturer's instructions. The quantity and quality of extracted RNA were measured using a SpectraMax ABS Plus spectrometer (Molecular Devices, CA, USA). All RNA samples were diluted to 1 μg. RT-qPCR was performed using the iScript cDNA synthesis kit (Bio-Rad, Hercules, CA, USA). Subsequently, real-time PCR was conducted using the SsoAdvanced Universal SYBR Green Supermix with CFX96™ System (Bio-Rad). Expression of each gene was normalized to the housekeeping gene, gapdh (ΔΔCq). Primer sequences used in experiments are listed in Supp table 4.

5.21. Metabolomic analysis

To extract metabolites for GC–MS analysis, each fecal sample was weighed and diluted in ice-cold 100 % methanol to a final concentration of 30 mg/mL. After centrifugation at 15,000×*g* for 5 min at 4 °C, the supernatant was filtered through a 0.2-μm polyvinylidene fluoride syringe filter. Aliquots of 0.2 mL of the filtered supernatant were concentrated in a vacuum concentrator and retained at −80 °C prior to derivatization. The extract was derivatized with 30 μL of 20 mg/mL methoxyamine hydrochloride in pyridine for 90 min at 30 °C and then 50 μL of N,O-bis(trimethylsilyl)trifluoroacetamide (BSTFA) for 30 min at 60 °C. Fluoranthene was added as an internal standard to the extract. For analysis, a Thermo Trace 1310 GC was used coupled to a Thermo ISQ LT single quadrupole mass spectrometer (Waltham, MA, USA). A 60-m-long DB-5MS column with an internal diameter of 0.2 mm and a film thickness of 0.25 μm (Agilent, Santa Clara, CA, USA) was used for the separation of metabolites. The sample was injected at 300 °C with a split ratio of 1:60 and a helium split flow of 7.5 mL/min. The metabolites were separated with a constant flow of 1.5 mL helium at an oven ramp of 5 °C/min, starting from 50 °C (held for 2 min) to 180 °C (held for 8 min), then to 210 °C (held for 2.5 min), and finally to 325 °C (held for 10 min). The mass spectra were acquired over a scan range of 35–650 m/z at an acquisition rate of 5 spectra per second using electron impact ionization. The ion source temperature was set to 270 °C. Thermo Xcalibur software was used for automated peak detection and identification of metabolites by matching their mass spectra and retention indices with those in the NIST Mass Spectral Search Program (version 2.0, Gaithersburg, MD, USA). Finally, the metabolite data were normalized based on the intensity of the internal standard, fluoranthene.

5.22. Metagenomic analysis

Fecal samples of each group were collected on the 7th day of DSS administration, and gDNA was extracted using the DNeasy PowerSoil Pro Kit (Qiagen, Hilden, Germany). Subsequently, the V3-V4 region of the 16s rRNA genes was amplified using the extracted DNA sample (V4 amplicon primer set: forward, 515F, 5′-TCGTCGGCAGCGTCAGATGTGTATAAGAGACAGGTGCCAGCMGCCGCGGTAA-3′; reverse, 806R, 5′-GTCTCGTGGGCTCGGAGATGTGTATAAGAGACAGGGACTACHVGGGTWTCTAAT-3′), and next-generation sequencing was performed using the Illumina® iSeq 100 (Illumina, Inc., CA, USA). Fastq files obtained from iSeq-100 paired-end sequencing data were analyzed using Mothur (v. 1.44.3). The Shannon and Chao indices of bacterial alpha diversity were analyzed using a nonparametric one-way analysis of difference ($p < 0.05$), the Kruskal–Wallis test, and Tukey's post hoc analysis. Welch's *t*-test was used to compare the differences in the relative abundance of bacterial composition. The weighted and unweighted UniFrac metrics of bacterial beta diversity were calculated based on the OTU table and the phylogenetic tree. The results were visualized using a principal coordinate analysis (PCoA) plot. PCoA plots were generated based on the weighted and unweighted UniFrac distances of the fecal microbiome of each group with distinct clustering.

5.23. Correlation analysis for metagenome and metabolome

The correlation between the microbiota and metabolites was conducted using the microbiome and metabolome integrative analysis pipeline (M2IA) (http://m2ia.met-bioinformatics.cn) for metabolome and microbiome correlation analysis (Ni et al., 2020). Different amounts of microbial communities were analyzed by genus and microbiome-metadata correlation analysis. The Spearman correlation coefficients were calculated using a pairwise correlation analysis method between differential microbiota and metabolites.

5.24. Statistical analysis

C. elegans lifespan and killing assay data were graphed using SigmaPlot 12.0 (Systat Software Inc.) and analyzed using the Kaplan–Meier method, and the significance of differences between survival curves was determined using the log-rank test (STATA6; STATA, TX, USA). Other analysis data were statistically graphed and analyzed using GraphPad Prism 9.5.0 (GraphPad software, USA). The significance level of the statistical analyses was set at p values < 0.05 (* or #), <0.01 (** or ##), <0.001(*** or ###), and <0.0001 (**** or ####). Group comparisons were performed using either one-way or two-way analysis of variance (ANOVA), depending on the experimental design. One-way ANOVA was applied when comparing three or more groups with a single factor, while two-way ANOVA was used for experiments involving two independent variables. To control for type I error in multiple comparisons, Tukey's honestly significant difference (HSD) post hoc test was applied following each ANOVA. All data are presented as mean ± standard deviation (SD).

CRediT authorship contribution statement

Anna Kang: Writing – original draft, Methodology, Investigation, Formal analysis, Conceptualization, Visualization, Software, Writing – review & editing. **Ju Young Eor:** Writing – original draft, Methodology, Investigation, Formal analysis, Conceptualization. **Junbeom Lee:** Writing – original draft, Methodology, Investigation, Formal analysis, Conceptualization. **Min-Jin Kwak:** Writing – review & editing, Visualization, Software, Methodology. **Daniel Junpyo Lee:** Writing – review & editing, Visualization, Software, Methodology, Data curation. **Eunsol Seo:** Writing – review & editing, Visualization, Software, Methodology. **Woong Ji Lee:** Writing – review & editing, Visualization, Software, Methodology. **Seon-hui Son:** Writing – review & editing, Visualization,

Software, Methodology. **Minho Song:** Visualization, Software, Methodology. **Jun-Mo Kim:** Visualization, Software, Methodology. **Hyung Wook Kim:** Visualization, Software, Methodology. **Jungwoo Yang:** Visualization, Software, Methodology. **Sangnam Oh:** Writing – review & editing, Supervision, Project administration, Investigation, Conceptualization. **Younghoon Kim:** Writing – review & editing, Supervision, Project administration, Investigation, Funding acquisition, Conceptualization.

Ethics approval and consent to participate

Not applicable.

Consent for publication

Not applicable.

Declaration of competing interest

The authors declare that they have no known competing financial interests or personal relationships that could have appeared to influence the work reported in this paper.

Acknowledgments

This study was supported by the National Research Foundation of Korea Grant, funded by the Korean government (MEST) (NRF-2021R1A2C3011051, Korea), by the Korea government (MSIT) (No. RS-2023-00218476, Korea), and by the Korea Institute of Planning and Evaluation for Technology in Food, Agriculture, Forestry and Fisheries (IPET-321037-5, Korea).

Appendix A. Supplementary data

Supplementary data to this article can be found online at https://doi.org/10.1016/j.crfs.2025.101051.

Data availability

Data will be made available on request.

References

Belovicova, K., Bogi, E., Csatlosova, K., Dubovicky, M., 2017. Animal tests for anxiety-like and depression-like behavior in rats. Interdiscip. Toxicol. 10 (1), 40–43. https://doi.org/10.1515/intox-2017-0006.

Bonaz, B., Bazin, T., Pellissier, S., 2018. The vagus nerve at the interface of the microbiota-gut-brain axis. Front. Neurosci. 12, 336468.

Brenner, S., 1974. The GENETICS of CAENORHABDITIS elegans. Genetics 77 (1), 71–94. https://doi.org/10.1093/genetics/77.1.71.

Cai, W., Pierzynowska, K., Stiernborg, M., Xu, J., Nilsson, I.A.K., Svensson, U., et al., 2024. Multispecies synbiotics alleviate dextran sulfate sodium (DSS)-induced colitis: effects on clinical scores, intestinal pathology, and plasma biomarkers in male and female mice. Clinical Nutrition ESPEN 63, 74–83. https://doi.org/10.1016/j.clnesp.2024.06.011.

Caldwell, K.A., Willicott, C.W., Caldwell, G.A., 2020. Modeling neurodegeneration in Caenorhabditis elegans. Disease Models & Mechanisms 13 (10). https://doi.org/10.1242/dmm.046110.

Chen, Y., Si, J-m, Liu, W-l, Cai, J-t, Du, Q., Wang, L-j, et al., 2007. Induction of experimental acute ulcerative colitis in rats by administration of dextran sulfate sodium at low concentration followed by intracolonic administration of 30% ethanol. J. Zhejiang Univ. - Sci. B 8 (9), 632–637. https://doi.org/10.1631/jzus.2007.B0632.

Choi, H., Mun, D., Ryu, S., Kwak, M.J., Kim, B.K., Park, D.J., et al., 2023. Molecular characterization and functionality of rumen-derived extracellular vesicles using a Caenorhabditis elegans animal model. J. Anim. Sci. Technol. 65 (3), 652. https://doi.org/10.5187/jast.2022.e124.

Chu, H., Du, C., Yang, Y., Feng, X., Zhu, L., Chen, J., et al., 2022. MC-LR aggravates liver lipid metabolism disorders in obese mice fed a high-fat diet via PI3K/AKT/mTOR/SREBP1 signaling pathway. Toxins 14 (12), 833.

Cryan, J.F., O'Riordan, K.J., Cowan, C.S., Sandhu, K.V., Bastiaanssen, T.F., Boehme, M., et al., 2019. The microbiota-gut-brain axis. Physiol. Rev. 99 (4), 1877–2013. https://doi.org/10.1152/physrev.00018.2018.

Dhabhar, F.S., 2014. Effects of stress on immune function: the good, the bad, and the beautiful. Immunol. Res. 58 (2), 193–210. https://doi.org/10.1007/s12026-014-8517-0.

Dong, L., Dong, F., Guo, P., Li, T., Fang, Y., Dong, Y., et al., 2025. Gut microbiota as a new target for hyperuricemia: a perspective from natural plant products. Phytomedicine 138, 156402. https://doi.org/10.1016/j.phymed.2025.156402.

Forth, E., Buehner, B., Storer, A., Sgarbossa, C., Milev, R., Meyyappan, A.C., 2023. Systematic review of probiotics as an adjuvant treatment for psychiatric disorders. Frontiers in Behavioral Neuroscience 17. https://doi.org/10.3389/fnbeh.2023.1111349.

Fung, T.C., Olson, C.A., Hsiao, E.Y., 2017. Interactions between the microbiota, immune and nervous systems in health and disease. Nat. Neurosci. 20 (2), 145–155.

Gao, Y., Zhang, S., Aili, T., Yang, J., Jia, Z., Wang, J., et al., 2022. Dual signal light detection of beta-lactoglobulin based on a porous silicon bragg mirror. Biosens. Bioelectron. 204, 114035.

Gareau, M.G., 2016. Chapter eleven - cognitive function and the microbiome. In: Cryan, J.F., Clarke, G. (Eds.), International Review of Neurobiology, vol. 131. Academic Press, pp. 227–246.

Goodwin, G.M., Stein, D.J., 2021. Generalised anxiety disorder and depression: contemporary treatment approaches. Adv. Ther. 38 (Suppl. 2), 45–51. https://doi.org/10.1007/s12325-021-01859-8.

Gould, T.D., Dao, D.T., Kovacsics, C.E., 2009. The open field test. Mood and Anxiety Related Phenotypes in Mice: Characterization Using Behavioral Tests, pp. 1–20.

Goya, M.E., Xue, F., Sampedro-Torres-Quevedo, C., Arnaouteli, S., Riquelme-Dominguez, L., Romanowski, A., et al., 2020. Probiotic Bacillus subtilis protects against α-synuclein aggregation in *C. elegans*. Cell Rep. 30 (2), 367-80. e7.

Goyache, I., Yavorov-Dayliev, D., Milagro, F.I., Aranaz, P., 2024. Caenorhabditis elegans as a screening model for probiotics with properties against metabolic syndrome. Int. J. Mol. Sci. 25 (2), 1321.

Han, S., Elnar, A., Lim, C., Kim, G.B., 2023. Complete genome sequence of bacteriocin-producing Ligilactobacillus salivarius B4311 isolated from fecal samples of broiler chicken with anti-listeria activity. J. Anim. Sci. Technol. https://doi.org/10.5187/jast.2023.e40.

Hu, D., Wan, L., Chen, M., Caudle, Y., LeSage, G., Li, Q., et al., 2014. Essential role of IL-10/STAT3 in chronic stress-induced immune suppression. Brain Behav. Immun. 36, 118–127. https://doi.org/10.1016/j.bbi.2013.10.016.

Huang, Y., Xu, Z., Xiong, S., Sun, F., Qin, G., Hu, G., et al., 2018. Repopulated microglia are solely derived from the proliferation of residual microglia after acute depletion. Nat. Neurosci. 21 (4), 530–540.

Huang, Y.Y., Wu, Y.P., Jia, X.Z., Lin, J., Xiao, L.F., Liu, D.M., et al., 2022. Lactiplantibacillus plantarum DMDL 9010 alleviates dextran sodium sulfate (DSS)-induced colitis and behavioral disorders by facilitating microbiota-gut-brain axis balance. Food Funct. 13 (1), 411–424. https://doi.org/10.1039/d1fo02938j.

Huang, L., Li, Y., Tang, R., Yang, P., Zhuo, Y., Jiang, X., et al., 2024a. Bile acids metabolism in the gut-liver axis mediates liver injury during lactation. Life Sci. 338, 122380.

Huang, L., Luo, S., Liu, S., Jin, M., Wang, Y., Zong, X., 2024b. Comparative multiomics analyses reveal the breed effect on the colonic host–microbe interactions in pig. iMetaOmics 1 (1), e8.

Jaafar, M., Xu, P., Mageswaran, U.M., Balasubramaniam, S.D., Solayappan, M., Woon, J., et al., 2023. Dairy based-LAB improved constipation via increasing fecal bulk and decreasing concentration of fecal threonine while preserving colonic goblet cell count. J. Anim. Sci. Technol. https://doi.org/10.5187/jast.2023.e93.

Jo, H., Han, G., Kim, E.B., Kong, C., Kim, B.G., 2023. Effects of supplemental bacteriophage on the gut microbiota and nutrient digestibility of ileal-cannulated pigs. J. Anim. Sci. Technol. https://doi.org/10.5187/jast.2023.e96.

Kendler, K.S., Zachar, P., Craver, C., 2011. What kinds of things are psychiatric disorders? Psychol. Med. 41 (6), 1143–1150. https://doi.org/10.1017/S0033291710001844.

Kim, H., Shin, M., Ryu, S., Yun, B., Oh, S., Park, D.-J., et al., 2021. Evaluation of probiotic characteristics of newly isolated lactic acid bacteria from dry-aged Hanwoo beef. Food Science of Animal Resources 41 (3), 468.

Kim, J.Y., Kim, J.Y., Kim, H., Moon, E.C., Heo, K., Shim, J.J., et al., 2022. Immunostimulatory effects of dairy probiotic strains Bifidobacterium animalis ssp. lactis HY8002 and Lactobacillus plantarum HY7717. J. Anim. Sci. Technol. 64 (6), 1117. https://doi.org/10.5187/jast.2022.e84.

Kim, B., Kim, K., Xu, X., Lee, H., Pathiraja, D., Park, D.J., et al., 2023a. Complete genome and two plasmids sequences of Lactiplantibacillus plantarum L55 for probiotic potentials. J. Anim. Sci. Technol. 65 (6), 1341–1344. https://doi.org/10.5187/jast.2023.e37.

Kim, B., Meng, Z., Xu, X., Baek, S., Pathiraja, D., Choi, I.G., et al., 2023b. Complete genome sequence of Limosilactobacillus fermentum JNU532 as a probiotic candidate for the functional food and feed supplements. J. Anim. Sci. Technol. 65 (1), 271. https://doi.org/10.5187/jast.2022.e91.

Kim, B., Xu, X., Lee, H., Pathiraja, D., Jae-Young, K., Choi, Y.H., et al., 2023c. Complete genome sequence of candidate probiotic Limosilactobacillus fermentuum KUFM407. J. Anim. Sci. Technol. https://doi.org/10.5187/jast.2023.e122.

Kim, J., Kim, H., Jeon, H.J., Jung, Y.H., Yang, J., 2024. Lacticaseibacillus casei IDCC 3451 strengthen digestibility of plant-based proteins in mice. Probiotics and Antimicrobial Proteins 16 (3), 927–935.

Kraeuter, A.K., Guest, P.C., Sarnyai, Z., 2019. The Y-maze for assessment of spatial working and reference memory in mice. Methods Mol. Biol. 1916, 105–111.

Kumar, A., Baruah, A., Tomioka, M., Iino, Y., Kalita, M.C., Khan, M., 2020. Caenorhabditis elegans: a model to understand host–microbe interactions. Cell. Mol. Life Sci. 77, 1229–1249.

Kumaree, K.K., Prasanth, M.I., Sivamaruthi, B.S., Kesika, P., Tencomnao, T., Chaiyasut, C., et al., 2023. Lactobacillus paracasei HII01 enhances lifespan and promotes neuroprotection in Caenorhabditis elegans. Sci. Rep. 13 (1), 16707.

Kwak, M.J., Chae, K.S., Kim, J.N., Whang, K.Y., Kim, Y., 2023. Dietary effects of melatonin on growth performance by modulation of protein bioavailability and behavior in early weaned rats and pigs. J. Anim. Sci. Technol. 65 (5), 1053–1064. https://doi.org/10.5187/jast.2023.e44.

Lee, D., Goh, T.W., Kang, M.G., Choi, H.J., Yeo, S.Y., Yang, J., et al., 2022. Perspectives and advances in probiotics and the gut microbiome in companion animals. J. Anim. Sci. Technol. 64 (2), 197. https://doi.org/10.5187/jast.2022.e8.

Li, J., Chen, Y., Zhang, S., Zhao, Y., Gao, D., Xing, J., et al., 2025. Purslane (Portulaca oleracea L.) polysaccharide attenuates carbon tetrachloride-induced acute liver injury by modulating the gut microbiota in mice. Genomics 117 (1), 110983. https://doi.org/10.1016/j.ygeno.2024.110983.

Liu, X., Du, Z.R., Wang, X., Sun, X.R., Zhao, Q., Zhao, F., et al., 2022. Polymannuronic acid prebiotic plus Lacticaseibacillus rhamnosus GG probiotic as a novel synbiotic promoted their separate neuroprotection against Parkinson's disease. Food Res. Int. 155, 111067.

Liu, W., Han, Y., An, J., Yu, S., Zhang, M., Li, L., et al., 2025. Alternation in sequence features and their influence on the anti-inflammatory activity of soy peptides during digestion and absorption in different enzymatic hydrolysis conditions. Food Chem. 471, 142824.

Lueptow, L.M., 2017. Novel object recognition test for the investigation of learning and memory in mice. J. Vis. Exp. 126. https://doi.org/10.3791/55718.

Lupien, S.J., Juster, R.P., Raymond, C., Marin, M.F., 2018. The effects of chronic stress on the human brain: from neurotoxicity, to vulnerability, to opportunity. Front. Neuroendocrinol. 49, 91–105. https://doi.org/10.1016/j.yfrne.2018.02.001.

McIntyre, G., Wright, J., Wong, H.T., Lamendella, R., Chan, J., 2021. Effects of FUdR on gene expression in the *C. elegans* bacterial diet OP50. BMC Res. Notes 14 (1), 207.

Minhas, P.S., Latif-Hernandez, A., McReynolds, M.R., Durairaj, A.S., Wang, Q., Rubin, A., et al., 2021. Restoring metabolism of myeloid cells reverses cognitive decline in ageing. Nature 590 (7844), 122–128.

Munezero, O., Cho, S., Kim, I.H., 2023. The effects of synbiotics-glyconutrients on growth performance, nutrient digestibility, gas emission, meat quality, and fatty acid profile of finishing pigs. J. Anim. Sci. Technol. https://doi.org/10.5187/jast.2023.e52.

Ni, Y., Yu, G., Chen, H., Deng, Y., Wells, P.M., Steves, C.J., et al., 2020. M2IA: a web server for microbiome and metabolome integrative analysis. Bioinformatics 36 (11), 3493–3498. https://doi.org/10.1093/bioinformatics/btaa188.

Obata, Y., Pachnis, V., 2016. The effect of microbiota and the immune system on the development and organization of the enteric nervous system. Gastroenterology 151 (5), 836–844.

Oh, Y.J., Lee, J., Lim, S.K., Kwon, M.S., Lee, S., Choi, S.P., et al., 2022a. Complete genome sequence of probiotic Lactobacillus johnsonii 7409N31 isolated from a healthy Hanwoo calf. J. Anim. Sci. Technol. https://doi.org/10.5187/jast.2022.e98.

Oh, S.H., Kim, I.S., Kim, G.I., Kim, J.A., Moon, Y.S., Jang, J.C., et al., 2022b. Intestinal microbial composition changes induced by Lactobacillus plantarum GBL 16, 17 fermented feed and intestinal immune homeostasis regulation in pigs. J. Anim. Sci. Technol. 64 (6), 1184. https://doi.org/10.5187/jast.2022.e89.

Papassotiropoulos, A., Fountoulakis, M., Dunckley, T., Stephan, D.A., Reiman, E.M., 2006. Genetics, transcriptomics, and proteomics of Alzheimer's disease. J. Clin. Psychiatr. 67 (4), 652.

Park, M.R., Ryu, S., Maburutse, B.E., Oh, N.S., Kim, S.H., Oh, S., et al., 2018. Probiotic Lactobacillus fermentum strain JDFM216 stimulates the longevity and immune response of Caenorhabditis elegans through a nuclear hormone receptor. Sci. Rep. 8 (1), 7441. https://doi.org/10.1038/s41598-018-25333-8.

Park, S., Kim, J.A., Jang, H.J., Kim, D.H., Kim, Y., 2023a. Complete genome sequence of functional probiotic candidate Lactobacillus amylovorus CACC736. J. Anim. Sci. Technol. 65 (2), 473. https://doi.org/10.5187/jast.2022.e85.

Park, S., Son, S., Park, M., Kim, D.H., Kim, Y., 2023b. Complete genome sequence of Latilactobacillus curvatus CACC879 and its functional probiotic properties. J. Anim. Sci. Technol. https://doi.org/10.5187/jast.2023.e50.

Pu, X., Sheng, S., Fu, Y., Yang, Y., Xu, G., 2024. Construction of circRNA–miRNA–mRNA ceRNA regulatory network and screening of diagnostic targets for tuberculosis. Ann. Med. 56 (1), 2416604.

Ruan, Y., Yuan, P.-P., Li, P.-Y., Chen, Y., Fu, Y., Gao, L.-Y., et al., 2023. Tingli Dazao Xiefei Decoction ameliorates asthma in vivo and in vitro from lung to intestine by modifying NO–CO metabolic disorder mediated inflammation, immune imbalance, cellular barrier damage, oxidative stress and intestinal bacterial disorders. J. Ethnopharmacol. 313, 116503.

Ryu, S., Oh, S., Park, M.R., Lee, W.J., Yun, B., Choi, H.J., et al., 2019. Pathogenesis of Enterohemorrhagic Escherichia coli O157:H7 is mediated by the cytochrome P450 family in Caenorhabditis elegans animal model. Food Control 103, 182–185. https://doi.org/10.1016/j.foodcont.2019.03.036.

Ryu, S., Doo, H., Kim, E.S., Keum, G.B., Kwak, J., Pandey, S., et al., 2023. Complete genome sequence of Lactiplantibacillus plantarum strain GA_C_14 with potential characteristics applicable in the swine industry. J. Anim. Sci. Technol. https://doi.org/10.5187/jast.2023.e134.

Salminen, S., Collado, M.C., Endo, A., Hill, C., Lebeer, S., Quigley, E.M.M., et al., 2021. The International Scientific Association of Probiotics and Prebiotics (ISAPP) consensus statement on the definition and scope of postbiotics. Nat. Rev. Gastroenterol. Hepatol. 18 (9), 649–667. https://doi.org/10.1038/s41575-021-00440-6.

Sarowska, J., Choroszy-Król, I., Regulska-Ilow, B., Frej-Madrzak, M., Jama-Kmiecik, A., 2013. The therapeutic effect of probiotic bacteria on gastrointestinal diseases. Adv. Clin. Exp. Med. 22 (5), 759–766.

Shajib, M.S., Baranov, A., Khan, W.I., 2017. Diverse effects of gut-derived serotonin in intestinal inflammation. ACS Chem. Neurosci. 8 (5), 920–931. https://doi.org/10.1021/acschemneuro.6b00414.

Shin, M., Ban, O.H., Jung, Y., Yang, J., Kim, Y., 2021. Genomic characterization and probiotic potential of Lactobacillus casei IDCC 3451 isolated from infant faeces. Lett. Appl. Microbiol. 72 (5), 578–588.

Sonowal, R., Swimm, A., Sahoo, A., Luo, L., Matsunaga, Y., Wu, Z., et al., 2017. Indoles from commensal bacteria extend healthspan. Proc. Natl. Acad. Sci. 114 (36), E7506–E7515. https://doi.org/10.1073/pnas.1706464114.

Tissenbaum, H.A., 2015. Using *C. elegans* for aging research. Invertebr. Reprod. Dev. 59 (Suppl. 1), 59–63. https://doi.org/10.1080/07924259.2014.940470.

Umbrello, G., Esposito, S., 2016. Microbiota and neurologic diseases: potential effects of probiotics. J. Transl. Med. 14 (1), 298. https://doi.org/10.1186/s12967-016-1058-7.

Urrutia, A., García-Angulo, V.A., Fuentes, A., Caneo, M., Legüe, M., Urquiza, S., et al., 2020. Bacterially produced metabolites protect *C. elegans* neurons from degeneration. PLoS Biol. 18 (3), e3000638.

van Baarlen, P., Wells, J.M., Kleerebezem, M., 2013. Regulation of intestinal homeostasis and immunity with probiotic lactobacilli. Trends Immunol. 34 (5), 208–215. https://doi.org/10.1016/j.it.2013.01.005.

van de Wouw, M., Boehme, M., Lyte, J.M., Wiley, N., Strain, C., O'Sullivan, O., et al., 2018. Short-chain fatty acids: microbial metabolites that alleviate stress-induced brain-gut axis alterations. J Physiol. 596 (20), 4923–4944. https://doi.org/10.1113/jp276431.

Vanderhoof, J.A., 2001. Probiotics: future directions123. The American journal of clinical nutrition 73 (6). https://doi.org/10.1093/ajcn/73.6.1152S, 1152S-5S.

Vasquez, R., Oh, J.K., Song, J.H., Kang, D.K., 2022. Gut microbiome-produced metabolites in pigs: a review on their biological functions and the influence of probiotics. J. Anim. Sci. Technol. 64 (4), 671. https://doi.org/10.5187/jast.2022.e58.

Wang, P.Y.T., Caspi, L., Lam, C.K.L., Chari, M., Li, X., Light, P.E., et al., 2008. Upper intestinal lipids trigger a gut–brain–liver axis to regulate glucose production. Nature 452 (7190), 1012–1016. https://doi.org/10.1038/nature06852.

Wang, Y., Xie, Q., Zhang, Y., Ma, W., Ning, K., Xiang, J.-Y., et al., 2020. Combination of probiotics with different functions alleviate DSS-induced colitis by regulating intestinal microbiota, IL-10, and barrier function. Appl. Microbiol. Biotechnol. 104, 335–349.

Wang, X., Yang, Y., Zou, J., Li, Y., Zhang, X.G., 2022. Chondroitin sulfate E alleviates beta-amyloid toxicity in transgenic Caenorhabditis elegans by inhibiting its aggregation. Int. J. Biol. Macromol. 209 (Pt A), 1280–1287. https://doi.org/10.1016/j.ijbiomac.2022.04.124.

Wu, Y., Luo, Y., 2005. Transgenic *C. elegans* as a model in Alzheimer's research. Curr. Alzheimer Res. 2 (1), 37–45.

Xia, Y., Chen, Y., Wang, G., Yang, Y., Song, X., Xiong, Z., et al., 2020. Lactobacillus plantarum AR113 alleviates DSS-induced colitis by regulating the TLR4/MyD88/NF-κB pathway and gut microbiota composition. J. Funct.Foods 67, 103854. https://doi.org/10.1016/j.jff.2020.103854.

Yang, S., Deng, C., Li, Y., Li, W., Wu, Q., Sun, Z., et al., 2022. Complete genome sequence of Lactiplantibacillus plantarum ST, a potential probiotic strain with antibacterial properties. J. Anim. Sci. Technol. 64 (1), 183. https://doi.org/10.5187/jast.2022.e7.

Yoo, J.M., Mendoza, R.M., Hwang, I.C., Kang, D.K., 2022a. Whole genome sequence analysis of Ligilactobacillus agilis C7 isolated from pig feces revealed three bacteriocin gene clusters. J. Anim. Sci. Technol. 64 (5), 1008. https://doi.org/10.5187/jast.2022.e55.

Yoo, J., Lee, J., Zhang, M., Mun, D., Kang, M., Yun, B., et al., 2022b. Enhanced γ-aminobutyric acid and sialic acid in fermented deer antler velvet and immune promoting effects. J. Anim. Sci. Technol. 64 (1), 166. https://doi.org/10.5187/jast.2021.e132.

Yu, P., Ke, C., Guo, J., Zhang, X., Li, B., 2020. Lactobacillus plantarum L15 alleviates colitis by inhibiting LPS-mediated NF-κB activation and ameliorates DSS-induced gut microbiota dysbiosis. Front. Immunol. 11, 575173.

Zeng, M., Zou, Y., Shi, Z., Wang, J., Yang, Y., Bai, Y., et al., 2024. A broad-spectrum broth rapidly and completely repairing the sublethal injuries of Escherichia coli caused by freezing and lactic acid alone or in combination for accurate enumeration. LWT 201, 116219. https://doi.org/10.1016/j.lwt.2024.116219.

Zhou, M., Liu, X., Yu, H., Gong, J., 2021. Lactobacillus regulates Caenorhabditis elegans cell signaling to combat Salmonella infection. Front. Immunol. 12, 653205. https://doi.org/10.3389/fimmu.2021.653205.

Zhou, B., Jin, G., Pang, X., Mo, Q., Bao, J., Liu, T., et al., 2022. Lactobacillus rhamnosus GG colonization in early life regulates gut-brain axis and relieves anxiety-like behavior in adulthood. Pharmacol. Res. 177, 106090.

Zhu, Z., Gu, Y., Zeng, C., Yang, M., Yu, H., Chen, H., et al., 2022. Olanzapine-induced lipid disturbances: a potential mechanism through the gut microbiota-brain axis. Front. Pharmacol. 13, 897926.